Efficient Implementation of NOCI-MP2 using the Resolution of the Identity Approximation with Application to Charged Dimers and Long C-C Bonds in Ethane Derivatives

Journal:	*Journal of Chemical Theory and Computation*
Manuscript ID	ct-2018-00697r
Manuscript Type:	Article
Date Submitted by the Author:	09-Jul-2018
Complete List of Authors:	Yost, Shane; Texas State University San Marcos Head-Gordon, Martin; University of California, Berkeley, Chemistry

Efficient implementation of NOCI-MP2 using the resolution of the identity approximation with application to charged dimers and long C-C bonds in ethane derivatives

Shane R. Yost[†,‡,¶] and Martin Head-Gordon[*,‡,¶]

†*Department of Chemistry and Biochemistry, Texas State University, San Marcos TX 78666*

‡*Department of Chemistry, University of California, Berkeley CA 94720*

¶*Chemical Sciences Division, Lawrence Berkeley National Laboratory, Berkeley CA 94720*

E-mail: mhg@cchem.berkeley.edu

Abstract

An efficient implementation of the perturb-then-diagonalize non-orthogonal configuration interaction method with second order Møller-Plesset perturbation theory (NOCI-MP2) is presented. Relative to other low scaling multireference perturbation theories, NOCI-MP2 often requires a much smaller active space because of the use of non-orthogonal reference configurations. Reworking the NOCI-MP2 equations with the resolution of the identity (RI) approximation enables the method to have the same memory requirements and computational scaling as single reference RI-MP2. The working equations are extended to include single substitutions as required when the reference determinants do not satisfy the Hartree-Fock equations. A detailed computational algorithm is presented along with timings to establish the performance of the

implementation. NOCI-MP2 is applied to the binding energy and charge resonance energy in dication and monocation π dimers, as well as di-diamantane ethane, and hexaphenyl ethane. A well-defined set of non-orthogonal determinants are obtained using absolutely localized molecular orbitals (ALMOs), as solutions to the self-consistent field for molecular interactions (SCF-MI) equations corresponding to covalent and ionic determinants. Agreement with experimental information where available, and other multi-reference methods, is satisfactory, with the use of an 0.3 a.u. level shift to guard against large MP2 amplitudes. For di-diamantane ethane and hexaphenyl ethane, large dispersion forces help stabilize the molecules despite the steric repulsion. By contrast, in the case of hexaphenyl ethane, the energy penalty from the geometric distortion of the fragments significantly weakens the bond.

Introduction

Standard electronic structure methods, such as Kohn-Sham density functional theory (DFT) are able to treat most energy differences associated with non-covalent interactions, isomerization energies, atomization energies, and barrier heights in molecules with increasing accuracy.[1–5] However, striking degradation occurs for some classes of problems.[6] In fact, only high levels of wavefunction-based electronic structure theory can accurately describe chemical problems such as bond breaking,[7–9] avoided crossings,[10–12] antiferromagnetically coupled metal centers,[13–15] and polyradical systems.[16–18] In these cases, a single Hartree-Fock (HF) (or Kohn-Sham) determinant is not able to properly describe the electronic wavefunction because the mean field approximation is not adequate to describe a set of strongly correlated electrons. The exact full configuration interaction (FCI) method captures both strong correlation and weak correlations by composing the electronic wavefunction as a linear combination of all possible single determinants. However, FCI scales exponentially with the number of electrons when computed exactly. Therefore there is much research activity on methods that approximate FCI, such as the density matrix renormalization group,[19–21] FCI

quantum Monte-Carlo,[22–24] and related adaptive CI methods.[25–27]

Alternatively, approximate multireference (MR) electronic structure theories[28] are designed to enable the inclusion of just the essential configurations in the reference itself, which can therefore be dramatically more compact than either FCI or any accurate approximation. For instance, in lithium fluoride, a single reference description works well in the bonded region where the ionic configuration is dominant. Likewise, a covalent spin-polarized single configuration of two neutral atoms is adequate at dissociation. But at intermediate separations, the wavefunction has essential contributions ($> 25\%$) from both the ionic and covalent configurations, and is multireference in character. In an approximate MR theory the total wavefunction is then just a linear combination of these more dominant single reference wavefunctions. The most common method of this type is complete active space self-consistent field (CASSCF).[29,30] In CASSCF one defines a set of occupied and unoccupied orbitals as the active space, and the total wavefunction is then defined as a small FCI wavefunction in that active space. CASSCF computational costs increase exponentially with the size of the active space, which can be reduced by approximations that truncate the number of determinants,[31,32] in addition to the FCI approximations mentioned above.

While CASSCF is most widely used, there are other treatments of strong correlation worth mentioning. Spin-flip CAS (SF-CAS) methods is one alternative that has attracted recent interest.[33–35] Valence bond (VB) methods are another approach that captures essential electron correlations within a very compact pairing wavefunction. VB methods range from classical valence bond approaches[36,37] to exponential-scaling spin-coupled VB,[38] to its low scaling coupled cluster valence bond approximation,[8,39] to breathing orbital VB wavefunctions[40,41] that mix together two or more VB wavefunctions to capture resonance effects.

Alternatively, a very general approach to strong correlation is to variationally combine a set of determinants that are individually energy optimized. One early example are ionization energies corresponding to valence oxygen hole states in the tetrahedral CrO_4^{2-} ion,[42] where HF breaks spatial symmetry to localize the hole on a single O atom. Non-orthogonal CI

(NOCI) between the 4 symmetry broken solutions is a compact and natural description of such states.[42,43] The same authors explored a similar NOCI approach for describing magnetic interactions between localized spin centers, to obtain the coupling constants that enter the Heisenberg model Hamiltonian.[44] In general, NOCI can be performed[45,46] on as many SCF solutions as one can identify,[47] although typically the higher determinants are not true minima in Hilbert space. Alternatively, approaches can be developed to define those determinants that contribute to essential correlation (e.g. ionic and covalent determinants).[48] In all these approaches, since each determinant undergoes orbital relaxation, the final set of HF determinants are non-orthogonal because they do not share the same set of molecular orbitals. NOCI is the reference of interest in this work.

Beyond the strong or essential correlation is the remaining weak or dynamic correlation. For simple problems, dynamic correlation is efficiently captured by well-established single reference methods such as coupled cluster (CC) theory[49] and Møller-Plesset (MP) perturbation theory.[50] From a CASSCF reference, there are many different methods that correct for the effects of weak correlation using either coupled cluster theory[51,52] or perturbation theory[53,54] corrections to a multireference wavefunction problem. MRCC methods are capable of obtaining highly accurate results but the computational cost scales at least as the number of determinants in the MR wavefunction multiplied by the scaling of the coupled cluster approximation. Beginning from a classical VB starting point,[36] VBPT2 has been developed as a correction for dynamical correlation[55,56] that plays a role akin to CASPT2 corrections to CASSCF.

MRPT can be formulated as either a non-degenerate (diagonalize-then-perturb) or a quasi-degenerate (perturb-then-diagonalize) fashion. Diagonalize-then-perturb methods include the commonly used CASPT2 method[57] in which the PT expansion involves iterative N^5 steps to obtain the final energy. CASPT2 combines low computational cost with nearly quantitative accuracy. However, it requires expertise to select an appropriate active space and a suitable level shift for the PT2 correction.[58] For avoided crossings and conical intersec-

tions, one needs to use the multi-state CASPT2 approach, which involves M^2N^5 computational effort, where M is the number of state-averaged CAS states.[59] The n-electron valence states for multireference perturbation theory (NEVPT)[60,61] also uses the CASSCF reference wavefunction with a different definition of the zeroth order Hamiltonian, and has similar computational cost (it can even be lower when internally contracted). The state specific MRPT theory by Mukherjee and co-workers[51,62] uses a different perturbation expansion to avoid the need for an orbital level shift and is formally size extensive. However, the increased robustness comes with increased computational cost. Perturb-then-diagonalize approaches include methods like the generalized van Vleck perturbation theory (GVVPT2),[63,64] the effective valence shell Hamiltonian,[53] and the intermediate Hamiltonian method.[65] GVVPT2 is a more accurate and stable method, but more computationally expensive than the other perturb-then-diagonalize approaches.

Beginning from a NOCI reference rather than CASSCF, one perturb-then-diagonalize method that was introduced years ago[66] but not fully realized until recently is NOCI-MP2.[67,68] Note that only the most recently reported formulation of NOCI-MP2 is size-consistent.[68] In NOCI-MP2, each NOCI determinant is expanded to first order correction in Møller-Plesset perturbation theory. Both Hamiltonian and overlap matrix elements of the NOCI problem are corrected via MP theory before diagonalizing. The advantage of using the non-orthogonal approach is that orbital relaxation introduces some of the missing weak electronic correlation. This has been shown in both the NOCI[45,46] and breathing orbital valence bond approach[41,69] to yield improved results over their strictly orthogonal counterparts. Both NOCI and NOCI-MP2 methods can often use significantly smaller active space sizes[46,67,68] than conventional active space methods.

A main objective of this paper is to report the first efficient implementation of the NOCI-MP2 method with the inclusion of singles excitations, which therefore opens the way for large-scale testing and applications. The computational cost of NOCI-MP2 scales as $N_o^2N_v^3$ with a memory demand that scales as $N_o^2N_v^2$. The memory requirement is associated with storage

of the full set of two-electron integrals, and it can be reduced by employing the resolution of the identity (RI) approximation in the PT2 correction.[70,71] The RI approximation does not introduce significant errors with an appropriately chosen basis set, but can reduce the memory cost to $N_v N_{aux}$. The methodological part of this paper will summarize the working equations of NOCI-MP2, which are extended to include contributions from single excitations. This permits use of non-Hartree-Fock determinants (i.e. which do not satisfy the Brillouin condition) within the NOCI reference. We next focus on introducing the RI approximation within the NOCI-MP2 framework and present the algorithms used to evaluate the steps that are important for efficient evaluation. Finally, we discuss how the computation of the off diagonal matrix elements scale with basis set size when compared to the RI-MP2 method.

The results presented in this paper have three separate components. The first part involves assessment of the observed computational cost of the NOCI-MP2 implementation as a function of molecular size, relative to single reference RI-MP2. The second part is a short study of antiferromagnetically coupled dimer dications and radical monocation dimers. These species are examples of multicenter long-bond complexes (about 3.7 Å for $TCNE^{-\bullet}$-$TCNE^{-\bullet}$) that are attracting interest in the context of both novel chemical bonding and possible relevance to organic materials.[72,73] The third part is a NOCI-MP2 study of the unusually long C-C single bond in the sterically crowded di-diamantane ethane and hexaphenyl ethane molecules. While alkanes normally have C-C single bond lengths of roughly 1.54 Å, the di-diamantane molecule was synthesized and characterized by crystallography as having a C-C single bond that is 1.65 Å. Chemical bonding in these compounds can be viewed as a tradeoff between Pauli repulsion between the bulky side groups (which forces lengthening and destabilization of the bond), and attractive London dispersion which provides compensating stabilization. However, this interpretation has been recently challenged,[74] with an alternative explanation in terms of small radical stabilization energy. Regardless of the details of interpretation, di-diamantane and hexaphenyl ethane can be viewed as models for how these effects play out in more complex supramolecular systems.[75]

Theory

Here we present the equations and algorithms for the RI approximation within the size consistent version of NOCI-MP2. The notation we use is described in Table 1. For simplicity, we use spin orbitals in the equations and algorithms, but of course the implementation is accomplished in terms of (unrestricted) spatial orbitals.

Table 1: Summary of index conventions.

Notation	Description
i, j, k, l	occupied spin orbital
a, b, c, d	virtual spin orbital
p, q, r, s	any spin orbital
$\tilde{i}, \tilde{j}, \tilde{k}, \tilde{l}$	occupied corresponding spin orbital
P, Q	auxiliary basis function
superscript A, B	NOCI state
N	number of basis functions
N_o	number of occupied spin orbitals
N_v	number of virtual spin orbitals
N_{aux}	number of auxiliary basis functions
$S_{\tilde{p}\tilde{q}}$	$\langle {}^A\psi_{\tilde{p}} \vert {}^B\psi_{\tilde{q}} \rangle$

NOCI-MP2 Ansatz

We refer the reader to previous work on the NOCI-MP2 method for the derivation of the size consistent formulation.[68] In this work we present what was previously called version 2 of the NOCI-MP2 method outlined in ref. 68, because this version includes the contribution of the MP2 overlap in the final set of equations. There is no significant computational cost difference between the two different size consistent variations of NOCI-MP2, because the MP2 overlap is freely obtained during the computation of the Hamiltonian. Version 1, also size-consistent, is obtained simply by removing some terms from version 2, and thus is a special case of the theory presented below. 68

In this paper we will introduce extra terms in the expansion of the wavefunction corresponding to singles amplitudes, which are non-zero only if the occupied-virtual block of

the Fock matrix is non-zero. In earlier work 66–68 the different NOCI determinants are all chosen to be solutions to the HF equation. Each NOCI state is made up of a set of canonical orbitals that fully diagonalize the Fock matrix. In the results section below, we will use other computational tools to find solutions to modified HF equations that do not fully diagonalize the Fock matrix. It is important to consider singles excitations for these cases because they are no longer strictly zero. Of course, if a NOCI determinant does fully diagonalize its Fock matrix, then all of the single excitation terms can be ignored in the NOCI-MP2 computation.

Given a set of NOCI determinants, $\{|^A\Psi\rangle\}$, that are expanded out to their first order correction in MP perturbation theory, $|^A\Psi\rangle = |^A\Psi^{(0)}\rangle + |^A\Psi^{(1)}\rangle$, then the size consistent NOCI-MP2 ansatz is:

$$\langle {}^A\Psi|\hat{H}|{}^B\Psi\rangle = \langle {}^A\Psi^{(0)}|\hat{H}|{}^B\Psi^{(0)}\rangle + \frac{1}{2}\left(\langle {}^A\Psi^{(0)}|\hat{H}|{}^B\Psi^{(1)}\rangle + \langle {}^A\Psi^{(1)}|\hat{H}|{}^B\Psi^{(0)}\rangle\right) \tag{1}$$

$$\langle {}^A\Psi|{}^B\Psi\rangle = \langle {}^A\Psi^{(0)}|{}^B\Psi^{(0)}\rangle + \frac{1}{2}\left(\langle {}^A\Psi^{(0)}|{}^B\Psi^{(1)}\rangle + \langle {}^A\Psi^{(1)}|{}^B\Psi^{(0)}\rangle\right) \tag{2}$$

The first order overlap term and the second order Hamiltonian term are defined as

$$\begin{aligned}\langle {}^A\Psi^{(0)}|\hat{H}|{}^B\Psi^{(1)}\rangle = {} & \frac{1}{4}t_{ij}^{ab}\left(E_{HF}^A + E_{MP2}^A\right)\langle {}^A\Psi^{(0)}|{}^B\Psi_{ij}^{ab}\rangle + \frac{1}{4}F_k^c t_{ij}^{ab}\langle {}^A\Psi_k^c|{}^B\Psi_{ij}^{ab}\rangle + \frac{1}{16}\langle kl\|cd\rangle t_{ij}^{ab}\langle {}^A\Psi_{kl}^{cd}|{}^B\Psi_{ij}^{ab}\rangle \\ & + t_i^a\left(E_{HF}^A + E_{MP2}^A\right)\langle {}^A\Psi^{(0)}|{}^B\Psi_i^a\rangle + F_k^c t_i^a\langle {}^A\Psi_k^c|{}^B\Psi_i^a\rangle + \frac{1}{4}\langle kl||cd\rangle t_i^a\langle {}^A\Psi_{kl}^{cd}|{}^B\Psi_i^a\rangle\end{aligned} \tag{3}$$

$$\langle {}^A\Psi^{(0)}|{}^B\Psi^{(1)}\rangle = \frac{1}{4}t_{ij}^{ab}\langle {}^A\Psi^{(0)}|{}^B\Psi_{ij}^{ab}\rangle + t_i^a\langle {}^A\Psi^{(0)}|{}^B\Psi_i^a\rangle \tag{4}$$

In the above equations, and henceforth, the t-amplitudes (and orbital energies) refer to the first order expansion of determinant B: $|^B\Psi^{(1)}\rangle = \sum_{ia} t_i^a|^B\Psi_i^a\rangle + \sum_{ijab} t_{ij}^{ab}|^B\Psi_{ij}^{ab}\rangle$; we suppress the state labels because only one determinant is referred to, although each NOCI determinant has its own first order amplitudes.

To evaluate the overlap terms between the molecular wavefunctions we rotate the occupied orbitals into the biorthogonal corresponding orbital basis.[76] The corresponding orbital

basis is formed by performing a singular value decomposition, SVD, on the occupied block of the overlap matrix

$$\mathbf{O}_{\mathrm{MO}} = (\mathbf{C}^A_{\mathrm{MO}})^T \mathbf{O}_{\mathrm{AO}} \mathbf{C}^B_{\mathrm{MO}} \tag{5}$$

$\mathbf{C}^X_{\mathrm{MO}}$ and $\mathbf{O}_{\mathrm{AO}}$ are the molecular orbital (MO) coefficients for state X and the atomic orbital (AO) overlap matrix, respectively. SVD of the occupied-occupied block of the MO overlap matrix $\mathbf{O_{occ}}$ yields

$$\mathbf{O}_{occ} = \mathbf{UsV} \tag{6}$$

The singular values, $S_{\tilde{j}}$, obtained from the SVD are the individual overlaps between the corresponding $\tilde{j}^{\mathrm{th}}$ occupied orbitals in state A and B. Only the occupied block of the molecular orbitals needs to be biorthogonalized to evaluate the NOCI-MP2 matrix elements. The overlap between the two determinants is then just a product of these overlaps, $O_{\mathrm{HF}} = \langle {}^A\Psi^{(0)} | {}^B\Psi^{(0)} \rangle = \prod_{\tilde{i}} S_{\tilde{i}}$. From the unitary matrices $\mathbf{U}$ and $\mathbf{V}$ we obtain the corresponding molecular orbitals

$$\begin{aligned} \tilde{C}^A_{\sigma\tilde{i}} &= \sum_j C^A_{\sigma j} U_{j\tilde{i}} \\ \tilde{C}^B_{\sigma\tilde{i}} &= \sum_j C^B_{\sigma j} V_{j\tilde{i}} \end{aligned} \tag{7}$$

Using the corresponding MOs we define the overlap quantities, $S_{\tilde{p}\tilde{q}}$, that are used to solve $\langle A | B^{ab}_{ij} \rangle$ and $\langle A^{cd}_{kl} | B^{ab}_{ij} \rangle$ and are given in the bottom of Table 1. We use the accented indices only for the occupied corresponding orbitals. Within the corresponding orbital basis we can rewrite Eqs (3) and (4) as

$$\begin{aligned} \langle {}^A\Psi^{(0)} | \hat{H} | {}^B\Psi^{(1)} \rangle = H_{\mathrm{sing}} &+ \sum_{\tilde{i}\tilde{j}ab} \frac{1}{2} t^{ab}_{\tilde{i}\tilde{j}} \left(E^A_{\mathrm{HF}} + E^A_{\mathrm{MP2}} \right) \frac{S_{\tilde{i}a} S_{\tilde{j}b}}{S_{\tilde{i}} S_{\tilde{j}}} O_{\mathrm{HF}} \\ &+ \sum_{\tilde{i}\tilde{j}ab} \sum_{\tilde{k}c} \frac{1}{4} F^c_{\tilde{k}} t^{ab}_{\tilde{i}\tilde{j}} \langle {}^A\Psi^c_{\tilde{k}} | {}^B\Psi^{ab}_{\tilde{i}\tilde{j}} \rangle + \sum_{\tilde{i}\tilde{j}ab} \sum_{\tilde{k}\tilde{l}cd} \frac{1}{16} \langle \tilde{k}\tilde{l} || cd \rangle t^{ab}_{\tilde{i}\tilde{j}} \langle {}^A\Psi^{cd}_{\tilde{k}\tilde{l}} | {}^B\Psi^{ab}_{\tilde{i}\tilde{j}} \rangle \end{aligned} \tag{8}$$

$$H_{\text{sing}} = \sum_{\tilde{i}a} t_{\tilde{i}}^{a} \left(E_{\text{HF}}^{A} + E_{\text{MP2}}^{A} \right) \frac{S_{\tilde{i}a}}{S_{\tilde{i}}} O_{\text{HF}} + \sum_{\tilde{i}\tilde{k}ac}^{\tilde{i}\neq\tilde{k}} F_{\tilde{k}}^{c} t_{\tilde{i}}^{a} \frac{S_{\tilde{i}a} S_{c\tilde{k}}}{S_{\tilde{i}} S_{\tilde{k}}} O_{\text{HF}} + \sum_{\tilde{i}ac} F_{\tilde{i}}^{c} t_{\tilde{i}}^{a} \frac{S_{ab}^{\tilde{i}}}{S_{\tilde{i}}} O_{\text{HF}}$$
$$+ \sum_{\tilde{k}\tilde{l}cd} \sum_{\tilde{i}a}^{\tilde{i}\neq\tilde{k},\tilde{l}} \frac{1}{4} \langle \tilde{k}\tilde{l} || cd \rangle t_{\tilde{i}}^{a} \frac{S_{\tilde{i}a} S_{\tilde{l}d} S_{c\tilde{k}}}{S_{\tilde{i}} S_{\tilde{l}} S_{\tilde{k}}} O_{\text{HF}} + \sum_{\tilde{i}\tilde{l}cd} \sum_{a} \frac{1}{2} \langle \tilde{i}\tilde{l} || cd \rangle t_{\tilde{i}}^{a} \frac{S_{\tilde{l}d} S_{ac}^{\tilde{i}}}{S_{\tilde{l}} S_{\tilde{i}}} O_{\text{HF}} \tag{9}$$

$$\langle {}^{A}\Psi^{(0)} | {}^{B}\Psi^{(1)} \rangle = \sum_{\tilde{i}\tilde{j}ab} \frac{1}{2} t_{\tilde{i}\tilde{j}}^{ab} \frac{S_{\tilde{i}a} S_{\tilde{j}b}}{S_{\tilde{i}} S_{\tilde{j}}} O_{\text{HF}} + \sum_{\tilde{i}a} t_{\tilde{i}}^{a} \frac{S_{\tilde{i}a}}{S_{\tilde{i}}} O_{\text{HF}} \tag{10}$$

The singles terms from Eq. (9) are computed in a straight forward manner. The singles amplitude, $t_{\tilde{i}}^{a}$, can be stored on disk, unlike the doubles amplitude, $t_{\tilde{i}\tilde{j}}^{ab}$. Likewise, all of the rotated matrix elements in the corresponding orbital basis are formed and stored on disk. The overall computation of Eq. (9) is on the order of $N_v^2 N_o$. The rest of this section will be focused on the computation of the last two terms in Eq. (8). The overlap matrix elements with excitations in state A and state B depend on how many of the occupied orbital indices in state A and state B are the same. When there are two excitations in both states the the three different cases are

Case 1: $\tilde{i} \neq \tilde{l}/\tilde{k}, \tilde{j} \neq \tilde{l}/\tilde{k}$

$$\sum_{\tilde{i}\tilde{j}ab} \sum_{\tilde{k}\tilde{l}cd} \frac{\langle \tilde{k}\tilde{l} || cd \rangle S_{c\tilde{k}} S_{d\tilde{l}} t_{\tilde{i}\tilde{j}}^{ab} S_{\tilde{i}a} S_{\tilde{j}b} O_{\text{HF}}}{4 S_{\tilde{k}} S_{\tilde{l}} S_{\tilde{i}} S_{\tilde{j}}} - \sum_{\tilde{i}\tilde{j}ab} \sum_{\tilde{l}cd} \frac{\langle \tilde{i}\tilde{l} || cd \rangle S_{c\tilde{i}} S_{d\tilde{l}} t_{\tilde{i}\tilde{j}}^{ab} S_{\tilde{i}a} S_{\tilde{j}b} O_{\text{HF}}}{4 S_{\tilde{i}} S_{\tilde{l}} S_{\tilde{i}} S_{\tilde{j}}}$$
$$+ \sum_{\tilde{i}\tilde{j}ab} \sum_{cd} \frac{\langle \tilde{i}\tilde{j} || cd \rangle S_{c\tilde{i}} S_{d\tilde{j}} t_{\tilde{i}\tilde{j}}^{ab} S_{\tilde{i}a} S_{\tilde{j}b} O_{\text{HF}}}{4 S_{\tilde{i}} S_{\tilde{j}} S_{\tilde{i}} S_{\tilde{j}}} \tag{11}$$

Case 2: $\tilde{i} = \tilde{k}, \tilde{j} \neq \tilde{l}/\tilde{k}$

$$\sum_{\tilde{i}\tilde{j}ab} \sum_{\tilde{l}cd} \frac{\langle \tilde{i}\tilde{l} || cd \rangle S_{d\tilde{l}} t_{\tilde{i}\tilde{j}}^{ab} S_{\tilde{j}b} S_{ca}^{\tilde{i}} O_{\text{HF}}}{4 S_{\tilde{l}} S_{\tilde{j}} S_{\tilde{i}}} - \sum_{\tilde{i}\tilde{j}ab} \sum_{cd} \frac{\langle \tilde{i}\tilde{j} || cd \rangle S_{d\tilde{j}} t_{\tilde{i}\tilde{j}}^{ab} S_{\tilde{j}b} S_{ca}^{\tilde{i}} O_{\text{HF}}}{4 S_{\tilde{j}} S_{\tilde{j}} S_{\tilde{i}}} \tag{12}$$

Case 3: $\tilde{i} = \tilde{k}, \tilde{j} = \tilde{l}$

$$\sum_{\tilde{i}\tilde{j}ab} \sum_{cd} \frac{\langle \tilde{i}\tilde{j}||cd\rangle S_{ac}^{\tilde{i}\tilde{j}} S_{bd}^{\tilde{i}\tilde{j}} t_{\tilde{i}\tilde{j}}^{ab} O_{\mathrm{HF}}}{4 S_{\tilde{i}} S_{\tilde{j}}} \tag{13}$$

The extra terms for Cases 1 and 2 are due to the sums not being restricted over situations like $\tilde{j} = \tilde{l}$. While not restricting the sums introduces extra terms that need to be computed, we will show that the low computational scaling can only be achieved by unrestricting the sums. The projected overlap terms in Cases 2 and 3 are defined as

$$S_{ac}^{\tilde{i}} = S_{ac} - \sum_{\tilde{k}\neq\tilde{i}} \frac{S_{a\tilde{k}} S_{\tilde{k}c}}{S_{\tilde{k}}} \tag{14}$$

$$S_{ac}^{\tilde{i}\tilde{j}} = S_{ac} - \sum_{\tilde{k}\neq\tilde{i},\tilde{j}} \frac{S_{a\tilde{k}} S_{\tilde{k}c}}{S_{\tilde{k}}} \tag{15}$$

Equations (8)-(13) define the specifics of the NOCI-MP2 off-diagonal Hamiltonian and overlap matrix elements. The diagonal matrix elements are just the MP2 energy for the Hamiltonian and 1.0 for the overlap. All of these equations assume that the SVD of $\mathbf{O}_{occ}$ does not include any zero singular values, i.e. $S_{\tilde{k}} \neq 0$. We will not give the specific equations for the cases when $S_{\tilde{k}} = 0$ or is near 0. These equations require expanding the sum over occupied indices into a sum over occupied orbitals with a non-zero $S_{\tilde{k}}$ and a sum over $S_{\tilde{k}}$ less than a threshold value. We use 10^{-4} as the threshold because dividing by numbers smaller than $(10^{-4})^4$ can yield numerically unstable results.

The extra term, $\sum_{\tilde{i}\tilde{j}ab} \sum_{\tilde{k}c} \frac{1}{4} F_{\tilde{k}}^{c} t_{\tilde{i}\tilde{j}}^{ab} \langle {}^{A}\Psi_{\tilde{k}}^{c} | {}^{B}\Psi_{\tilde{i}\tilde{j}}^{ab} \rangle$, that is needed for cases when the Fock matrix is not diagonal is rewritten as

$$\begin{aligned} \sum_{\tilde{i}\tilde{j}ab} \sum_{\tilde{k}c} \frac{1}{4} F_{\tilde{k}}^{c} t_{\tilde{i}\tilde{j}}^{ab} \frac{S_{\tilde{i}a} S_{\tilde{j}b} S_{c\tilde{k}}}{S_{\tilde{i}} S_{\tilde{j}} S_{\tilde{k}}} O_{\mathrm{HF}} - \sum_{\tilde{i}\tilde{j}ab} \sum_{kc} \frac{1}{2} F_{\tilde{i}}^{c} t_{\tilde{i}\tilde{j}}^{ab} \frac{S_{\tilde{i}a} S_{\tilde{j}b} S_{c\tilde{i}}}{S_{\tilde{i}} S_{\tilde{j}} S_{\tilde{i}}} O_{\mathrm{HF}} \\ + \sum_{\tilde{i}\tilde{j}ab} \sum_{c} \frac{1}{2} F_{\tilde{i}}^{c} t_{\tilde{i}\tilde{j}}^{ab} \frac{S_{\tilde{j}b} S_{ac}^{\tilde{i}}}{S_{\tilde{j}} S_{\tilde{i}}} O_{\mathrm{HF}} \end{aligned} \tag{16}$$

These two terms are computed in the same way as Eqs. (11) and (12). The specifics of which will be outlined bellow.

Finally we need to define the two-electron integrals within the RI approximation. The main advantage of the RI approximation is that it greatly reduces the memory demand, and slightly reduces the computational cost. Within the RI approximation a two-electron integral becomes

$$\langle ij|ab\rangle \approx \sum_{PQ} \frac{(ia|P)(Q|jb)}{(P|Q)} = \sum_{Q} B^Q_{ia} B^Q_{jb} \tag{17}$$

$$B^Q_{pq} = \sum_P (pq|P)(P|Q)^{-\frac{1}{2}} \tag{18}$$

So instead of storing the four index two-electron integral on disk or in memory the three index B amplitudes defined in Eq. (18) can be stored on disk or in memory. We will show later that use of the RI approximation requires only $N_v N_{aux}$ elements of the B tensor to be stored in memory. Due to use of the corresponding orbitals, the two electron integrals need to be rotated into the corresponding orbital basis. The t amplitudes in Eqs. (8)-(10) then become:

$$t^{ab}_{\tilde{i}\tilde{j}} = \sum_{ij} V_{i\tilde{i}} t^{ab}_{ij} V_{j\tilde{j}} = \sum_{ij} \frac{V_{i\tilde{i}} B^Q_{ia} B^Q_{jb} V_{j\tilde{j}} - V_{i\tilde{i}} B^Q_{ib} B^Q_{ja} V_{j\tilde{j}}}{\epsilon_i + \epsilon_j - \epsilon_a - \epsilon_b} \tag{19}$$

$$t^{a}_{\tilde{i}} = \sum_{i} \frac{V_{i\tilde{i}} F_{ia}}{\epsilon_i - \epsilon_a} \tag{20}$$

In the next section we will present the final set of RI equations through combining Eqs. (8)-(13) with Eq. (19) for a low scaling algorithm. First we will mention that if the t amplitudes correspond to the ket state then the two-electron integrals in Eq. (8) correspond to the bra state, or vice versa. This means that the NOCI-MP2 equations require at least twice the number of B tensors as normal RI-MP2. The NOCI-MP2 algorithm can still scale similarly to RI-MP2, but will in general have a larger prefactor.

NOCI-MP2 Algorithm

This section focuses on the equations and algorithm used for the fast NOCI-MP2 algorithm within the RI approximation. The first step is to combine Eq. (10) with Eq. (19). The resulting equation is also used for the first term in Eq. (8), with the difference that it is multiplied by $(E^A_{\mathrm{HF}} + E^A_{\mathrm{MP2}})$. Using the RI approximation the MP2 overlap becomes

$$\sum_{ijab}\sum_{\tilde{i}\tilde{j}} \frac{S_{\tilde{i}a}S_{\tilde{j}b}V_{i\tilde{i}}t^{ab}_{ij}V_{j\tilde{j}}O_{\mathrm{HF}}}{2S_{\tilde{i}}S_{\tilde{j}}} = \sum_{ijab}\frac{1}{2}R_{ia}R_{jb}t^{ab}_{ij}O_{\mathrm{HF}} \tag{21}$$

$$R_{ia} = \sum_{\tilde{i}}\frac{V_{i\tilde{i}}S_{\tilde{i}a}}{S_{\tilde{i}}} \tag{22}$$

By pre-summing over the corresponding orbital indices (Eq. (22)) Eq. (21) scales as an RI-MP2 calculation with the slowest step being the formation of the t amplitudes. As we will see, with some reworking of the equations we can achieve the same scaling for all of the other terms in Eqs. (11)-(13). We can rewrite Eq. (11) using the same property of associativity in the summation indices to obtain the final set of equations for Case 1

$$\frac{O_{\mathrm{HF}}}{4}\sum_{klcd}\langle kl||cd\rangle Q_{ck}Q_{dl}\sum_{ijab}t^{ab}_{ij}R_{ia}R_{jb} - O_{\mathrm{HF}}\sum_{\tilde{i}}(\sum_{kc}\frac{U_{k\tilde{i}}S_{c\tilde{i}}}{S_{\tilde{i}}}(W1)_{kc})(\sum_{ia}\frac{V_{i\tilde{i}}S_{\tilde{i}a}}{S_{\tilde{i}}}(Z1)_{ia}) + \frac{O_{\mathrm{HF}}}{2}\sum_{\tilde{i}\tilde{j}}(X1)_{\tilde{i}\tilde{j}}(Y1)_{\tilde{i}\tilde{j}} \tag{23}$$

where

$$Q_{ai} = \sum_{\tilde{i}}\frac{U_{i\tilde{i}}S_{a\tilde{i}}}{S_{\tilde{i}}} \tag{24}$$

and

$$(W1)_{ic} = \sum_{ld}\langle il||cd\rangle Q_{dl}; \quad (Z1)_{ia} = \sum_{jb}t^{ab}_{ij}R_{jb} \tag{25}$$

and

$$(X1)_{\tilde{i}\tilde{j}} = \sum_{klcd}\frac{U_{k\tilde{i}}\langle kl||cd\rangle U_{l\tilde{j}}S_{c\tilde{i}}S_{d\tilde{j}}}{S_{\tilde{i}}S_{\tilde{j}}}; \quad (Y1)_{\tilde{i}\tilde{j}} = \sum_{ijab}\frac{V_{i\tilde{i}}t^{ab}_{ij}V_{j\tilde{j}}S_{\tilde{i}a}S_{\tilde{j}b}}{S_{\tilde{i}}S_{\tilde{j}}} \tag{26}$$

The second and third terms in Eq. (23) correct for the unrestricted summations over k and l. These summations should be restricted to not include i or j, but the calculation greatly benefits from being able to separate the summations. Specifically, if the first term in Eq. (11) has restricted sums, then that term scales at best as $N_o^4 N_v^2$. So even though extra terms with similar computational cost are added in, the overall cost is substantially reduced by unrestricting the sums. Similarly, Case 2 becomes

$$O_{\mathrm{HF}} \sum_{\tilde{i}ac} \frac{S^{\tilde{i}}_{ca}}{S_{\tilde{i}}} (\sum_{k} (W1)_{kc} U_{k\tilde{i}}) (\sum_{i} (Z1)_{ia} V_{i\tilde{i}}) - O_{\mathrm{HF}} \sum_{\tilde{i}\tilde{j}ac} \frac{S^{\tilde{i}}_{ca} (I2)^{c}_{\tilde{i}\tilde{j}} (L2)^{a}_{\tilde{i}\tilde{j}}}{S_{\tilde{i}}} \tag{27}$$

where

$$(I2)^{c}_{\tilde{i}\tilde{j}} = \sum_{kld} \frac{U_{k\tilde{i}} \langle \tilde{k} l || cd \rangle U_{l\tilde{j}} S_{d\tilde{j}}}{S_{\tilde{j}}}; \quad (L2)^{a}_{\tilde{i}\tilde{j}} = \sum_{ijb} \frac{V_{i\tilde{i}} t^{ab}_{ij} V_{j\tilde{j}} S_{\tilde{j}b}}{S_{\tilde{j}}} \tag{28}$$

For this case we need to form an intermediate three index quantity. This means that we will have cubic storage, though with a small prefactor since it scales as $N_o^2 N_v$. The size of these three index tensors are sometimes smaller than the largest two index tensors that are stored in memory due to the typically small size of N_o compared to N_v and N_{aux}.

In the case when the Fock matrix is not diagonal the terms, given in Eq. (16), need to be computed. The resulting terms when combining Eq. (16) and (19) are

$$\begin{aligned} \frac{O_{\mathrm{HF}}}{2} \sum_{\tilde{k}c} \frac{F^{c}_{\tilde{k}} S_{c\tilde{k}}}{S_{\tilde{k}}} \sum_{ijab} t^{ab}_{ij} R_{ia} R_{jb} - O_{\mathrm{HF}} \sum_{\tilde{i}} (\sum_{c} \frac{F^{c}_{\tilde{i}} S_{\tilde{i}c}}{S_{\tilde{i}}}) (\sum_{ia} \frac{V_{i\tilde{i}} S_{\tilde{i}a}}{S_{\tilde{i}}} (Z1)_{ia}) \\ + O_{\mathrm{HF}} \sum_{\tilde{i}ac} \frac{S^{\tilde{i}}_{ca} F^{c}_{\tilde{i}}}{S_{\tilde{i}}} (\sum_{i} (Z1)_{ia} V_{i\tilde{i}}) \end{aligned} \tag{29}$$

These contributions to the off-diagonal NOCI Hamiltonian scale by at least a factor of N less than their counterparts in Eqs. (23) and (27). Just like the additional terms in Eq. (9), all of the contributions from singles excitations are relatively cheap compared to the doubles excitations and are not the dominant factors in determining the overall time and computational scaling of the NOCI-MP2 method.

In computing the final term, Eq. (13), we cannot use Eq. (15) in the given compact form because it does not allow the terms to be refactored into a lower scaling form like in Eqs. (23) and (27). In order to reduce the number of coupled indices in Eq. (15) we define

$$S^{ac}_{\mathrm{Proj}} = S_{ac} - \sum_{k} \frac{S_{a\tilde{k}} S_{\tilde{k}c}}{S_{\tilde{k}}} \tag{30}$$

Using this, Eq. (15) can be written as

$$S^{\tilde{i}\tilde{j}}_{ab} = S^{ac}_{\mathrm{Proj}} + \frac{S_{a\tilde{i}} S_{\tilde{i}b}}{S_{\tilde{i}}} + \frac{S_{a\tilde{j}} S_{\tilde{j}b}}{S_{\tilde{j}}} \tag{31}$$

Now no more than two indices that are strictly coupled. Substituting this into Eq. 13 and expanding, we get four unique terms and the final set of equations

$$\begin{aligned} &\frac{O_{\mathrm{HF}}}{4} \sum_{ijab} \langle ij||ab\rangle t^{ab}_{ij} + O_{\mathrm{HF}} \sum_{\tilde{i}\tilde{j}a} \frac{(I3)^{a}_{\tilde{i}\tilde{j}} (L3)^{a}_{\tilde{i}\tilde{j}}}{S_{\tilde{i}} S^2_{\tilde{j}}} \\ &+ \frac{O_{\mathrm{HF}}}{4} \sum_{\tilde{i}\tilde{j}} \frac{(X3)_{\tilde{i}\tilde{j}} (Y3)_{\tilde{i}\tilde{j}}}{S^2_{\tilde{i}} S^2_{\tilde{j}}} + \frac{O_{\mathrm{HF}}}{2} \sum_{\tilde{i}\tilde{j}} \frac{(W3)_{\tilde{i}\tilde{j}} (Z3)_{\tilde{i}\tilde{j}}}{S^3_{\tilde{i}} S_{\tilde{j}}} \end{aligned} \tag{32}$$

where

$$(I3)^{a}_{\tilde{i}\tilde{j}} = \sum_{klcd} U_{k\tilde{i}} \langle kl||cd\rangle U_{l\tilde{j}} S^{ac}_{\mathrm{Proj}} S_{d\tilde{j}}; \quad (L3)^{a}_{\tilde{i}\tilde{j}} = \sum_{ijb} V_{i\tilde{i}} t^{ab}_{ij} V_{j\tilde{j}} S_{\tilde{j}b} \tag{33}$$

and

$$(X3)_{\tilde{i}\tilde{j}} = \sum_{klcd} U_{k\tilde{i}} \langle kl||cd\rangle U_{l\tilde{j}} S_{c\tilde{i}} S_{d\tilde{j}}; \quad (Y3)_{\tilde{i}\tilde{j}} = \sum_{ijab} V_{i\tilde{i}} t^{ab}_{ij} V_{j\tilde{j}} S_{\tilde{i}a} S_{\tilde{j}b} \tag{34}$$

and

$$(W3)_{\tilde{i}\tilde{j}} = \sum_{klcd} U_{k\tilde{i}} \langle kl||cd\rangle U_{l\tilde{j}} S_{c\tilde{i}} S_{d\tilde{i}}; \quad (Z3)_{\tilde{i}\tilde{j}} = \sum_{ijab} V_{i\tilde{i}} t^{ab}_{ij} V_{j\tilde{j}} S_{\tilde{i}a} S_{\tilde{i}b} \tag{35}$$

and

$$\langle ij||ab\rangle = \sum_{Q} ({}^{A}\bar{B}^{Q}_{ia}\, {}^{A}\bar{B}^{Q}_{jb} - {}^{A}\bar{B}^{Q}_{ja}\, {}^{A}\bar{B}^{Q}_{ib}) \tag{36}$$

where

$$ {}^{A}\bar{B}^{Q}_{ia} = \sum_{kc} {}^{A}B^{Q}_{kc} S^{ac}_{\mathrm{Proj}} \sum_{i} \frac{U_{i\tilde{i}} V_{k\tilde{i}}}{S_{\tilde{i}}} \tag{37} $$

We have defined a rotated two electron integral in Eq. (36), where the integral for state A is essentially rotated into the state B basis. Equations (21), (23), (27), and (32) are the set of working equations that need to be computed for the MP2 correction to the off diagonal matrix elements. All of these equations assume that the occupied-occupied and virtual-virtual blocks of the Fock matrix are diagonal.

Now that the working equations are defined, we present a sketch of the NOCI-MP2 algorithm within the RI approximation. The matrix elements we are looking for are between the zeroth order wavefunction of basis determinant A and the first order wavefunction of determinant B. The algorithm is broken up into three major steps: first the formation of Eqs. (18) and (37), followed by computing the contributions from Case 1, 2, and then 3.

In the first part of the algorithm, given in Figure 1, we create B^{Q}_{ia} in the same way as the RI-MP2 method,[77,78] the details of which we will not give here. The next step is to create and store Eq. (37) on disk. This step just involves rotating the virtual and occupied orbitals into the basis of the ket determinant. This scales as N^4 because we are rotating the three index quantity B^{Q}_{ia}.

Figure 1: Sketch for the formation of the B matrices used in the RI expansion to form the two-electron integrals.

	CPU	Disk
Form ${}^{A}B^{Q}_{ia}$, ${}^{B}B^{Q}_{ia}$	$N^2 N_v N_{aux}$	$N_o N_v N_{aux}$
Loop over k		
Read ${}^{B}B^{Q}_{kc}$		
${}^{B}\tilde{B}^{Q}_{kc} = \sum_c {}^{B}B^{Q}_{kc} S^{ac}_{\mathsf{Proj}}$	$N_o N_v^2 N_{aux}$	
Loop over i		
${}^{B}\bar{B}^{Q}_{ia} += (\sum_{\tilde{i}} \frac{U_{i\tilde{i}} V_{k\tilde{i}}}{S_{\tilde{i}}}) {}^{B}\tilde{B}^{Q}_{ka}$	$N_o^2 N_v N_{aux} + N_o^3$	$N_o N_v N_{aux}$

Next we compute Eqs. (10), (23), (27), and (29) using the algorithm sketched in Figure 2. The slowest scaling part of this step is the formation of the two-electron integrals ($N_o^2 N_v^2 N_{aux}$), which is the same as the slowest scaling part in the RI-MP2 method.[78] There

is another step that has fifth order scaling, but it scales as $N_o^3 N_v^2$.

As mentioned, one of the intermediate terms formed is a three index tensor. The price of storing these quantities on disk would be an excessive number of reads from disk. The number of seeks would scale as N_o^4, and the total data transfer would be $N_o^5 N_v$. Since this third rank tensor is also relatively small ($N_o^2 N_v$) we choose to store it in memory. For moderately large basis sets where $N_v >> N_o$ these three index tensors are not the most memory intensive terms. In the systems studied in this paper, over 600 basis functions, these tensors require less than 300 hundred megabytes of memory.

Figure 2: Sketch for the formation of the Hamiltonian contributions for Case 1 and Case 2, as well as the MP2 overlap term.

	CPU	Memory
Loop over i		
Read ${}^{A}B_{ia}^{Q}$, ${}^{B}B_{ic}^{Q}$		
Loop over j		
Read ${}^{A}B_{jd}^{Q}$, ${}^{B}B_{jb}^{Q}$		
Form t_{ij}^{ab},$\langle ij\|\|cd\rangle$	$N_o^2 N_v^2 N_{aux}$	N_v^2
$O_{\mathsf{MP2}} = \sum_{ab} t_{ij}^{ab} R_{ia} R_{jb} O_{\mathsf{HF}}$	$N_o^2 N_v^2$	
$C_1 += O_{\mathsf{MP2}}$		
$H_{\mathsf{MP2}} += O_{\mathsf{MP2}} * (E_{\mathsf{HF}} + E_{\mathsf{MP2}})$		
$C_2 += \sum_{cd} \langle ij\|\|cd\rangle Q_{ic} Q_{jd}$	$N_o^2 N_v^2$	
Form $(W1)_{ic}$,$(Z1)_{ia}$	$N_o^2 N_v^2$	$N_o N_v$
Form $(X1)_{\tilde{i}\tilde{j}}$,$(Y1)_{\tilde{i}\tilde{j}}$	$N_o^2 N_v + N_o^3 N_v^2$	$N_o N_v + N_o^2 N_v$
Form $(I2)_{\tilde{i}\tilde{j}}^{c}$,$(L2)_{\tilde{i}\tilde{j}}^{a}$	$N_o^2 N_v + N_o^3$	$N_o^2 + N_o^2 N_v$
$H_{\mathsf{MP2}} += C_1(\frac{C_2}{4} + \sum_{\tilde{k}c} \frac{F_{\tilde{k}}^{c} S_{\tilde{k}c}}{2 S_{\tilde{k}}})$		
$H_{\mathsf{MP2}} -= O_{\mathsf{HF}} \sum_{\tilde{i}} (\sum_{kc} \frac{U_{k\tilde{i}} S_{c\tilde{i}} (W1)_{kc}}{S_{\tilde{i}}} + \sum_{c} \frac{F_{\tilde{i}}^{c} S_{\tilde{i}c}}{S_{\tilde{i}}}) (\sum_{ia} \frac{V_{i\tilde{i}} S_{\tilde{i}a} (Z1)_{ia}}{S_{\tilde{i}}})$	$N_o^2 N_v$	
$H_{\mathsf{MP2}} += \sum_{\tilde{i}\tilde{j}} \frac{(X1)_{\tilde{i}\tilde{j}} (Y1)_{\tilde{i}\tilde{j}} O_{\mathsf{HF}}}{2}$	N_o^2	
$H_{\mathsf{MP2}} += \sum_{\tilde{i}ac} \frac{O_{\mathsf{HF}} S_{ca}^{\tilde{i}} (F_{\tilde{i}}^{c} + \sum_k (W1)_{kc} U_{k\tilde{i}}) (\sum_i (Z1)_{ia} V_{i\tilde{i}})}{S_{\tilde{i}}}$	$N_o N_v^2 + N_o^2 N_v$	
$H_{\mathsf{MP2}} -= \sum_{\tilde{i}\tilde{j}ac} \frac{S_{ca}^{\tilde{i}} (I2)_{\tilde{i}\tilde{j}}^{c} (L2)_{\tilde{i}\tilde{j}}^{a}}{S_{\tilde{i}}}$	$N_o^2 N_v^2$	

Finally we compute the last contribution to the Hamiltonian, Eq. (32) using the steps outlined in Figure 3. Despite the simple form in the original NOCI-MP2 method in Eq. (13) the new form required to optimally use the RI approximation takes just as long, if not longer, than the computation of Eqs. (23) and (27). This part of the matrix element is the most

computational expensive because there are three different two-electron integrals needed. In addition, the formation of Eq. 33 scales as $N_o^2 N_v^3$. The size of N_v and N_{aux} are typically similar, which is why these terms typically take the longest time to compute. Eq. (32) is almost always the largest contributor to the Hamiltonian matrix element due to the fact that the overlap between virtual orbitals in the bra and ket determinants, S_{ac}, are typically much larger than the occupied-virtual overlap, $S_{\tilde{i}a}$.

Figure 3: Sketch for the formation of Case 3 in the Hamiltonian.

	CPU	Memory
Loop over i		
Read ${}^A B^Q_{ia}$, ${}^B B^Q_{ic}$, ${}^B \bar{B}^Q_{ia}$		
Loop over j		
Read ${}^A B^Q_{jd}$, ${}^B B^Q_{jb}$, ${}^B \bar{B}^Q_{jb}$		
Form t^{ab}_{ij},$\langle ij\|\|cd\rangle$,$\langle ij\bar{\|}\|cd\rangle$	$N_o^2 N_v^2 N_{aux}$	N_v^2
Form $(I3)^a_{\tilde{i}\tilde{j}}$	$N_o^2 N_v^3 + N_o^3 N_v^2$	$N_o^2 N_v$
Form $(L3)^a_{\tilde{i}\tilde{j}}$	$N_o^3 N_v^2$	$N_o^2 N_v$
Form $(X3)_{\tilde{i}\tilde{j}}$,$(Y3)_{\tilde{i}\tilde{j}}$,$(W3)_{\tilde{i}\tilde{j}}$,$(Z3)_{\tilde{i}\tilde{j}}$	$N_o^3 N_v^2 + N_o^3 N_v$	N_o^2
$H_{\mathsf{MP2}} += \sum_{ab} \langle ij\|\|ab\rangle t^{ab}_{ij} \frac{O_{\mathsf{HF}}}{4}$	$N_o^2 N_v^2$	
$H_{\mathsf{MP2}} += \sum_{\tilde{i}\tilde{j}a} \frac{(I3)^a_{\tilde{i}\tilde{j}} (L3)^a_{\tilde{i}\tilde{j}} O_{\mathsf{HF}}}{S_{\tilde{i}} S^2_{\tilde{j}}}$	$N_o^2 N_v$	
$H_{\mathsf{MP2}} += \sum_{\tilde{i}\tilde{j}} \frac{(X3)_{\tilde{i}\tilde{j}} (Y3)^a_{\tilde{i}\tilde{j}} O_{\mathsf{HF}}}{4 S^2_{\tilde{i}} S^2_{\tilde{j}}} + \sum_{\tilde{i}\tilde{j}} \frac{(W3)_{\tilde{i}\tilde{j}} (Z3)^a_{\tilde{i}\tilde{j}} O_{\mathsf{HF}}}{2 S^3_{\tilde{i}} S_{\tilde{j}}}$	N_o^2	

We conclude this section by mentioning a few things about the implementation of the presented algorithm. As mentioned previously, we have assumed that all singular values, $S_{\tilde{i}}$, are greater than a threshold to avoid numerical instability problems. In practice the algorithm is modified by splitting up the sum into two different terms, one with $S_{\tilde{i}}$ greater than some threshold value and one term with $S_{\tilde{i}}$ smaller than that threshold value. This does not create any more computation, but does mean that there are a few more $\bar{B}^Q_{ia}$ matrices that must be stored on disk. In general, as the number of below-threshold singular values grows, the cost of the NOCI-MP2 method decreases because the sum over the corresponding orbitals becomes just a sum over one or two indices since the sum over $S_{\tilde{i}}$ greater than the threshold becomes zero. Therefore, what is presented here represents the worst case (largest possible amount of computation) for the NOCI-MP2 method.

To further increase the speed, we integrate out the spin, which creates a total of five unique non-zero cases for Eqs. (23)-(32). The reason there are five potential unique terms rather than three is because we have two different two-electron integrals multiplied together. Out of the five non-zero integrals only some contribute to all the cases; for example, if there are all alpha spins for one two-electron integral and all beta spins for the other two electron integral then only the first term in Eq. (23) is nonzero because the overlap integrals are zero for all other cases.

It is also worth mentioning that this method is easily parallelized over multiple CPUs. The computation of each Hamiltonian matrix element is independent of each other. Since the corresponding orbitals are also unique for a given bra-ket pair, it is only the atomic orbital two-center one-electron integrals from the RI expansion that are shared across all matrix elements (i.e. all processors). The code can then be easily parallelized over multiple processors based on the number of Hamiltonian matrix elements that need to be computed.

We have also implemented the frozen core approximation within the NOCI-MP2 method. The computational speed up is not as large as in the case of RI-MP2 because only the t_{ij}^{ab} amplitudes use the frozen core approximation. The other two-electron integral is not a part of the MP2 expansion, but instead arises because of the insertion of the identity used to solve the NOCI-MP2 Hamiltonian. We do not apply the frozen core approximation to this resolution of the identity because it introduces a larger error than the frozen core approximation in the MP2 method.

Results and Discussion

In this section, we discuss some timing comparisons against conventional RI-MP2, and two chemical applications of NOCI-MP2, including examples of larger molecules than was possible previously. The RI algorithm for the NOCI-MP2 method is implemented within a development version of the Q-Chem 5 quantum chemistry package[79] with OpenMP parallization.

All calculations were performed using a threshold value for $S_{\tilde{i}}$ of 0.001 and NOCI-MP2 v1[68] (i.e. neglecting the correction to the off-diagonal overlap matrix element that defined version 2). We then examine a number of singlet biradicaloid systems that require an electronic structure method capable of handling strong correlation.

The results for the biradicaloid systems use a damping or level shift term for t amplitudes based on the difference between the occupied and virtual orbital energies. We use this to guard against cases where the energy denominator in the t amplitudes approaches zero, which potentially leads to divergent amplitudes and second order energies. The parameter used for this damping is 0.3 Hartree, similar to the parameter that was determined to be optimal for regularized orbital optimized MP2.[80] In the sections below, we will discuss why this is used and the impact it has on the results.

Scaling

The timing of NOCI-MP2 with the RI approximation is compared to the corresponding RI-MP2 algorithm[78] within Q-Chem on a set of planar conjugated molecules, shown in Figure 4. We choose this test set to keep the density matrix denser than in the more standard test case of a set of linear alkanes, as well as to yield lower sparsity in AO basis matrix elements. The timing recorded for RI-NOCI-MP2 is for the computation of a single off-diagonal Hamiltonian matrix element. Because this is a perturb-then-diagonalize method all of the computational cost comes in forming the Hamiltonian and overlap in the NOCI basis. The timing of the overlap terms itself is not needed because they are obtained freely by just dividing the first term in Eq (8) by the total energy of the bra state.

In Figure 5 we plot the timing of a single off-diagonal Hamiltonian matrix element for RI-NOCI-MP2 and the timing to compute the RI-MP2 energy with respect to the basis set size. We use the aug-cc-pvdz basis set, which for our test set means we go from 192 to 770 basis functions. The slope for both of these methods does not quite reach 5 (asymptotically $N_o^2 N_v^2 N_{aux}$) on the log-log plot in Figure 5 reflecting two possible factors. First is the fact

Figure 4: The set of molecules used for timing calculations for RI-NOCI-MP2 and RI-MP2.

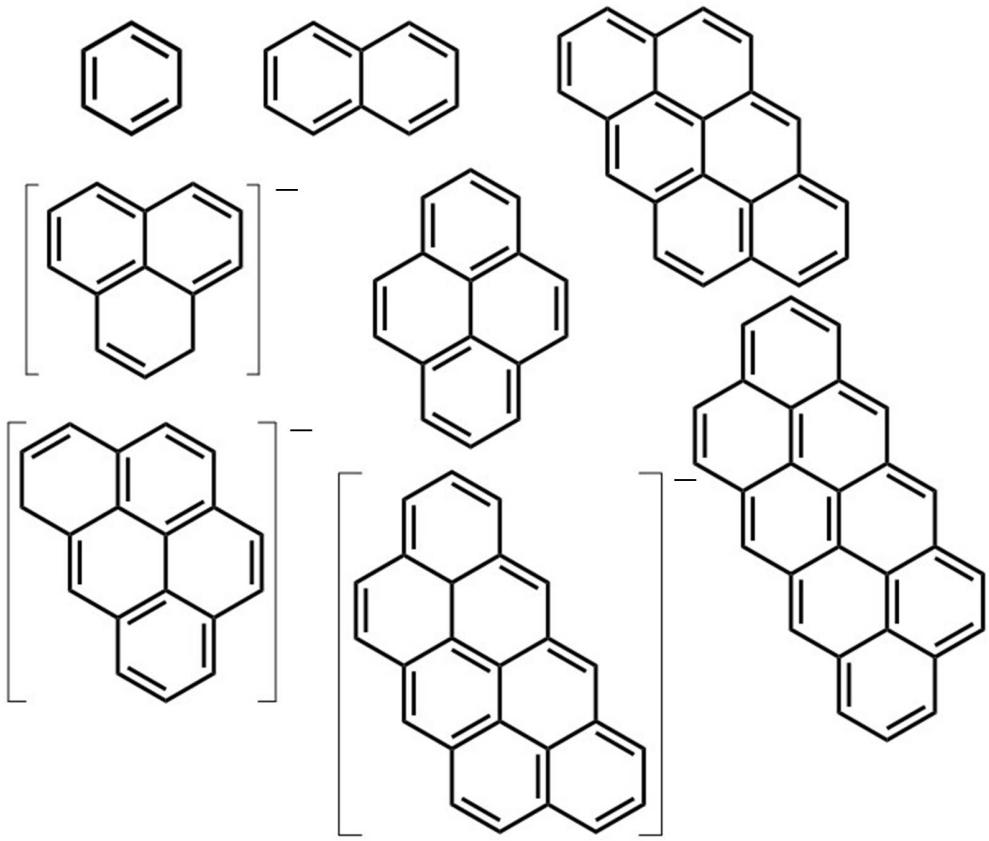

that the linear algebra associated with the rate-determining 5^{th} order steps executes faster as the problem size increases (approaching peak performance), and second is the fact that cubic and quartic scaling steps also make contributions to the timings. Both RI-MP2 and RI-NOCI-MP2 show similar scaling with respect to the size of the problem indicating that similar considerations apply to both algorithms. Similarly Figure 6 shows that RI-NOCI-MP2 and RI-MP2 display similar speed up over multiple processors. RI-NOCI-MP2 gains a little more than RI-MP2 with the increase in number of processors because RI-NOCI-MP2 has a larger ratio of computational vs. read/write time.

The prefactor associated with RI-NOCI-MP2 scaling ends up being roughly 10 times larger than RI-MP2. Part of this is due to the formation of the intermediates in Eqs. (33) and (36). Unrestricted RI-MP2 requires the formation of 3 different types of two-electron integrals; two same spin terms and the opposite spin term. For NOCI-MP2 there are those

Figure 5: Log-Log plot of the RI-NOCI-MP2 and RI-MP2 timings for the molecules shown in Figure 4 with respect to the number of basis functions. The RI-MP2 and RI-NOCI-MP2 scale a little lower than 5 because the asymptotic regime has not quite been reached for these problem sizes. Both calculations are executed presuming unrestricted orbitals, and were recorded on a 64 core node based on AMD Opteron 6134 processors running at a clock speed of 3.2 GHz. Both calculations were performed on a single processor.

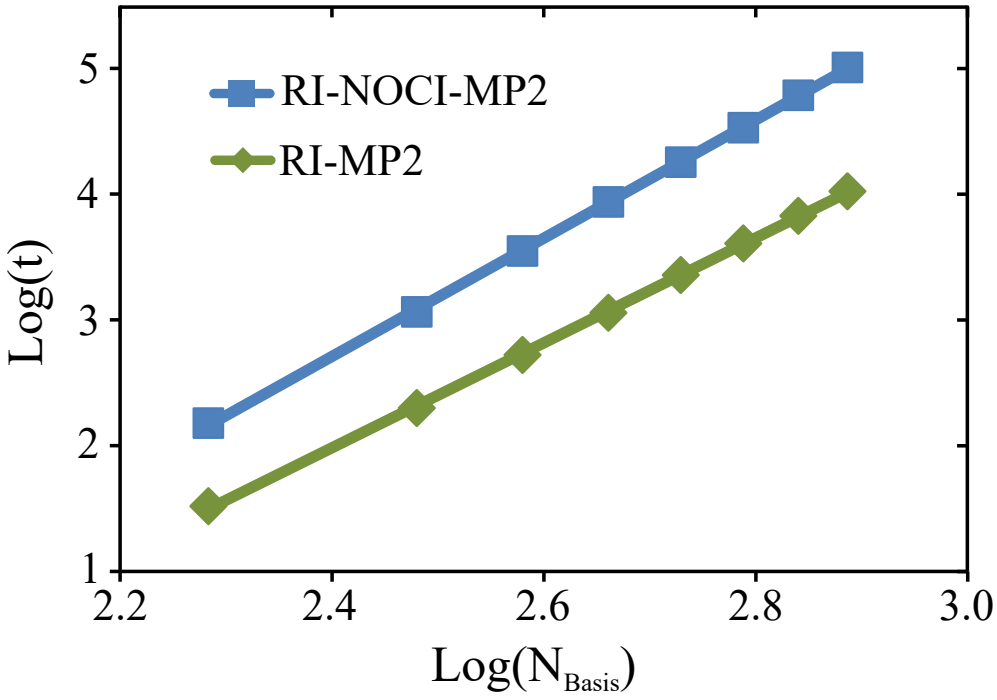

three cases for both of the spin integrated two-electron integrals $\langle kl||cd\rangle$ and t_{ij}^{ab} in Eq. (8). All of these extra terms add up to give roughly a factor of 10 times a conventional RI-MP2 calculation. In practice there are a number of ways to reduce the cost of a given matrix element by avoiding the computation of nearly zero terms based on the resulting overlap integrals, $S_{\tilde{ia}}$, and singular values, $S_{\tilde{i}}$, from the SVD in Eq. (5). These are utilized in the rest of the calculations presented in this paper, but Figures 5 and 6 use the slowest case scenario.

The other critical factor, so far ignored, in determining the computational cost of the NOCI-MP2 calculation is the rank of the NOCI matrix. The case of 4 determinants corresponds to the NOCI analog of a single spin-flip calculation and is appropriate for biradicaloids and single bond-breaking as treated in the following subsections. With the use of the sym-

Figure 6: Ratio of timing using N cores vs. one core for OpenMP parallized RI-MP2 and RI-NOCI-MP2. The black curve is a perfect parallization speedup. Both calculations are executed presuming unrestricted orbitals, and were recorded on a 64 core node based on AMD Opteron 6134 processors running at a clock speed of 3.2 GHz.

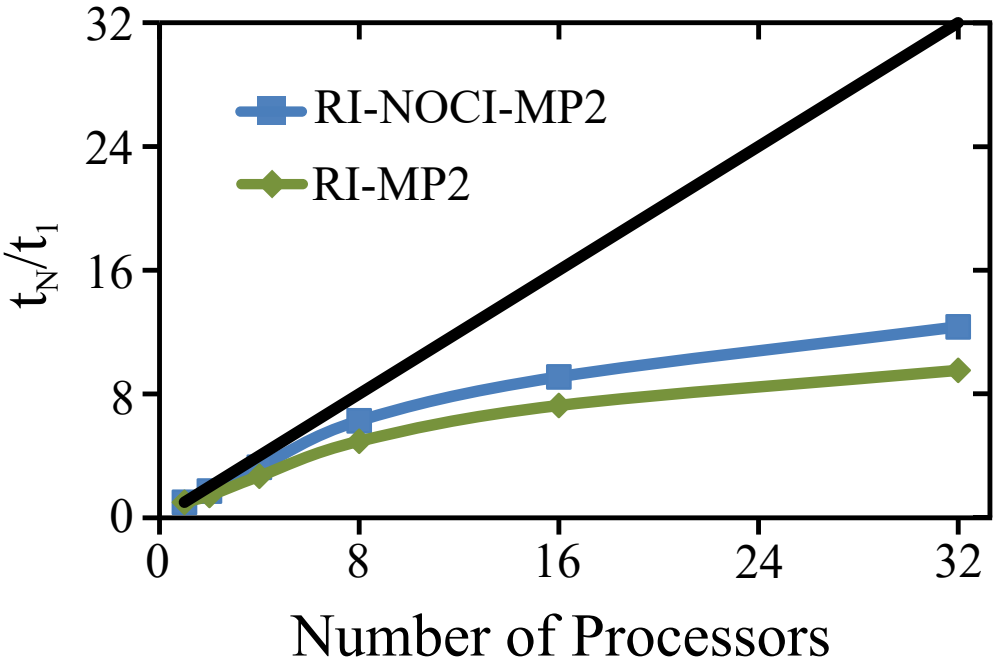

metry in the NOCI-MP2 Hamiltonian there are 3 diagonal and 8 off-diagonal elements to consider. The timing is therefore approximately 8.3 times longer than the single matrix element tests reported above. This common case then involves approximately 83 times more computation for the NOCI-MP2 correction than the RI-MP2 correction. Since we have excluded the SCF times, the overall computational cost increase for the complete NOCI-MP2 calculation versus RI-MP2 can be considerably less than this estimate. For example, a calculation with 692 basis functions on one processor the RI-NOCI-MP2 correction is 70 times longer than the RI-MP2 expansion. With the SCF time, the total RI-NOCI-MP2 calculation is 25 times longer than a RI-MP2 calculation.

Charged dimers

The recoupling of two π aromatic radicals, such as two ethene radical cations, can lead to a stacking complex with non-bonded contact distances that are shorter than a normal van

der Waals complex, yet much longer than a normal chemical bond. The resulting complex is biradicaloid in character, with a long, weak multicenter bond that reflects competition between stabilization due to recoupling of the two radical electrons, as well as dispersion interactions, countered by non-bonded contacts between other doubly occupied orbitals. If the radicals are charged, there is also significant electrostatic repulsion, which will typically render the complex meta-stable with respect to dissociation in the gas phase. Either way, these long, weak multicenter bonds require an electronic structure treatment capable of describing strong correlations because of their significant biradicaloid character.[81–83] Additionally dispersion interactions play a key role, and therefore a suitable electronic structure method must also include dynamic correlation.

To explore the performance of NOCI-MP2 for treating multi-center bonds in dication dimers, we must first specify the determinants that will be included in the reference NOCI calculation. One well-defined choice that seems appropriate is to obtain the covalent (radical) and ionic (closed shell) NOCI states using the absolutely localized molecular orbital (ALMO) method.[84–86] In the ALMO model, the MOs are constrained to be fragment block-diagonal such that AOs from one fragment cannot contribute to the MOs of any other fragment. This enables the optimization of constrained determinants, which correspond to well-defined covalent and ionic diabatic states. Due to the constraints, an ALMO determinant has non-zero occupied-virtual Fock matrix elements, and therefore requires inclusion of the single excitations in the MP2 treatment, as given in the theory section. Using the ALMO method we create 2 covalent (Monomer$^{+\bullet}$-Monomer$^{+\bullet}$) and 2 ionic (Monomer-Monomer^{2+}) determinants where the radical electrons are fragment localized into (nonorthogonal) orbitals on one monomer or the other. We pseudo-canonicalize the occupied-occupied and virtual-virtual block of the final MOs from the ALMO calculation in order to compute the MP2 correction to each of the 4 resulting determinants. This does not change the NOCI energies, but simplifies evaluation of the first order MP expansion of the wavefunction.

We first start with a simple model system of di-ethylene di-cation, plotted in Figure 7.

Figure 7: Dissociation curve in D_{2h} symmetry for ethylene dimer di-cation in the cc-pVTZ basis. There is a metastable minimum corresponding to weak 4-center inter-fragment bonding, although this minimum is unbound with respect to dissociation.

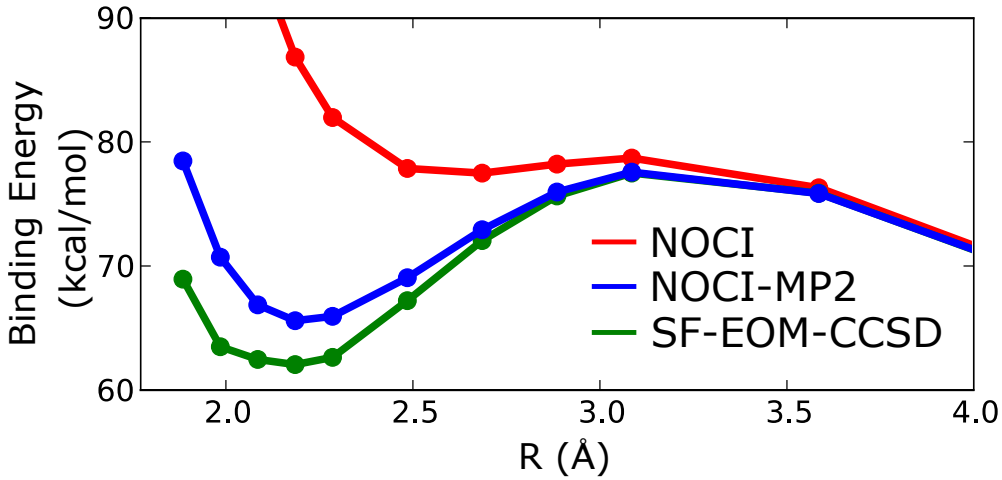

The D_{2h} geometry of di-ethylene dication is optimized using the ωB97X-D functional[87] with the cc-pVTZ basis set, and is given in the supporting information. The coordinates for each point on the curve shown in in Figure 7 are generated by rigidly pulling apart the ethylene cation radicals. We compute the ground state with SF-EOM-CCSD, NOCI, and NOCI-MP2 using the cc-pVTZ basis set. The SF-EOM-CCSD and NOCI-MP2 curves are corrected for basis set superposition error, while there is no basis set superposition error at the NOCI level because the molecular orbitals are restricted to one of the two monomers. To compute the basis set superposition error for NOCI-MP2 we use the basis set superposition error for single reference MP2 and remove the HF basis set superposition error.

Compared to SF-EOM-CCSD, NOCI-MP2 underbinds by about 3 kcal/mol, and shows very good qualitative agreement in the potential curves, by contrast with the NOCI method, which greatly underbinds the local minimum. A major reason for the good agreement between SF-EOM-CCSD and NOCI-MP2 is the inclusion of the singles amplitudes in the NOCI-MP2 perturbation theory expansion. Without singles, NOCI-MP2 underbinds by 15 kcal/mol and overestimates the bond distance by 0.3 Å.

One technical comment is in order. As mentioned above, there is an 0.3 a.u. damping or

level shift added to the energy denominators of the t amplitudes. This is most significant for short contacts i.e. equilibrium or shorter). The largest the HOMO and LUMO gap is over the entire curve is 0.2 Hartree and reaches values as small as 0.06 Hartree. Without damping, NOCI-MP2 overbinds by 12 kcal/mol, while it underbinds by 3 kcal/mol by adopting the level shift that has proved useful in OO-MP2. The character of the ground state also significantly changes without damping: the dominant ALMO NOCI states are the two radical ALMO states that spin-couple together to form the weak covalent bond, but for NOCI-MP2 without damping, the dominant ALMO NOCI states are the ionic states. Since the damped and undamped NOCI-MP2 results straddle the reference SF-EOM-CCSD results, one might infer that an optimal damping parameter (for this problem) would be slightly smaller than 0.3 a.u. However, we will not consider tuning the damping parameter or modifying its functional form here, as the present unbiased choice appears adequate.

Using the ALMO NOCI basis states makes it possible to further analyze the long multi-center bond that is formed. Assuming a simple covalent bond would imply that the two radical states are all that is needed to form the bond. However, if one uses just those two states then the NOCI-MP2 minimum is reduced by 18 kcal/mol. The barrier also decreases from 12 kcal/mol to 1 kcal/mol without the ionic states. This bonding may be viewed as an extreme case of the charge-shift bonding that has been identified in other molecules such as F_2 that have some diradicaloid character.[88,89] Other biradicaloid dimers with long inter-monomer separations will very likely exhibit the same character. Such systems have more typically been treated by CAS(2,2) wavefunctions which typically give delocalized active orbitals.

To compare with other multi-reference perturbation theory methods, like CASPT2, we model the tetracyano ethylene (TCNE) dimer di-anion, also in D_{2h} symmetry. In Table 2 we give the NOCI-MP2 results and the CASPT2 and RASPT2 results from reference 82. All of the values are computed with the 6-31+G* basis and corrected for basis set superposition error. NOCI-MP2 values are computed with geometries optimized using the

ωB97X-D functional and the 6-31+G* basis set. At each point along the potential energy scan the geometry is optimized while constraining the intermolecular separation distance. The geometries used as well as the raw data for NOCI-MP2 with and without the damping is given in the supporting information. For NOCI and NOCI-MP2 the 4 ALMO NOCI basis states are again used.

Due to lack of dispersion interactions, the di-anion dimer is completely unbound by the NOCI method and has no metastable state. The minimum for NOCI-MP2, given in Table 2, is 0.05Åless bound than RASPT2, which is significantly better than CASPT2 based on the similar sized active space CAS(2,2) results. However, NOCI-MP2 with the damped t amplitudes is less bound than by CASPT2 and RASPT2 methods. By contrast, without damping, the minimum is overbound (30 kcal/mol vs dissociation) with a barrier that is significantly too large (14 kcal/mol). The barrier and the minimum shift by roughly similar amounts (18 and 12 kcal/mol) because the damping has less impact on the barrier height and a larger impact on the minimum, because the singles amplitudes are the largest near the bonded region. The HOMO to LUMO energy difference is between 1.3-0.07 Hartree for the bonded region of the di-anion TCNE dimer. Overall, these results are broadly similar to the case of ethene dimer dication: without damping we over correlate, and the optimal result is somewhere between the damped and undamped results. Like the ethene dimer dication case, these results also suggest that there is scope for further investigation and optimization of the strategy for damping in the future.

Table 2: Meta-stable minimum and energy barriers for the di-anion TCNE dimer in the 6-31+G* basis for a variety of multi-reference perturbation theory methods. The CAS and RAS results are taken from reference 82. All energies are given in kcal/mol. Bond distances are given in Å

	NOCI-MP2	CAS(2,2)	CAS(6,4)	RAS(22,2,2;10,2,8)	RAS(22,2,2;8,4,8)
Minimum	48.4	34.8	37.9	37.3	36.7
Energy Barrier	2.28	9.43	7.02	5.31	6.14
Bond Distance	2.75	2.5	2.5	2.7	2.7

Just like in inorganic semiconductors, organic semiconductors exhibit increased conduc-

tance by doping with a small fraction of ionized molecules (i.e. holes). In these materials, the radical cation can form a dimer with a neutral molecule to delocalize the positive charge, and it is this monocation dimer that causes a significant increase in the charge mobility in the material.[90–92] To explore the use of NOCI-MP2 for aromatic dimer cations, we looked at the binding energy and the charge resonance energy for 4 examples (aniline, naphthalene, anthracene, and phenalenyl), and compare to gas phase experimental data where available.[93–95] Using the ALMO strategy for these species suggests that two diabatic configurations are natural: (Monomer$^{+\bullet}$-Monomer and Monomer-Monomer$^{+\bullet}$. These will give rise to two NOCI states associated with constructive and destructive interference between these localized charge diabatic determinants.

Since there is no long-range coulomb repulsion between the two monomers, the monocation dimers are bound with respect to dissociation in the gas phase: they represent a long multicenter interaction that is formally a half-bond. The ground state is not typically strong correlated (it is the delocalization of the odd electron or hole between the two monomers) and so single reference methods can do a good job at obtaining the binding energies (although hybrid functionals are essential in DFT to keep delocalization errors from being too large). Using the four state ALMO basis, the charge resonance energy (i.e. the excitation energy difference between the $\psi_{\pm} = \frac{1}{\sqrt{2}}\left(|A^{+}A\rangle \pm |AA^{+}\rangle\right)$ states) is freely obtained.

In table 3 we give the NOCI, NOCI-MP2, MP2, and DFT (using the accurate ωB97X-V hybrid[96]) calculations, and experimental binding energies and charge resonance energies. All of the computational values are corrected for basis set superposition error, and use the cc-pVTZ basis set. All of the geometries used for the dimers are given in the supporting information. As expected normal MP2 overbinds the π-stacked dimers compared to the DFT or experimental values: MP2 is known to overbind π stacking systems, as indicated by the benzene dimer,[97] DNA stacking complexes,[98] and related systems.[99] The difference between MP2 and the DFT results increases with the number of π electrons. This overbinding tendency will be directly reflected in the diagonal elements of the NOCI-MP2 method, which

would lead to overbinding in the absence of damping.

The binding of the cation-dimers can be viewed as having two main origins. One is the electrostatic/dispersion interactions, and the other is the splitting of the plus/minus combination of the localized ionic states given by the charge resonance energy. With the ALMO NOCI basis, the diagonal elements can tell us the impact of the electrostatic/dispersion interaction and the off-diagonal element determines the charge resonance energy. For example, the localized cation state ($|A^+A\rangle$) in naphthalene is bound by 6.45 kcal/mol at the MP2 level. This part of the binding is dominated by dispersion since without any dispersion, (the NOCI result), the state is unbound by 8 kcal/mol. The rest of the 10 kcal/mol binding energy is due to the weak one-electron bond formed in the ψ_+ state.

The damped NOCI-MP2 results in Table 3 are generally in quite good agreement with the ωB97X-V binding energy calculations, as well as the available experimental binding energies, with no deviation larger than 2 kcal/mol. The charge resonance energies predicted by damped NOCI-MP2 match up very well with the available experimental values, which also suggests that the off-diagonal matrix elements are quite accurate. One interesting subtlety is that in contrast to the experimental results, none of the dispersion including methods find that anthracene is less bound than naphthalene. Only with the NOCI method, where there are no dispersion interactions, is anthracene more bound. Comparing to experiments, it would seem that all methods (apart from NOCI, of course) over-estimate the importance of the dispersion interactions.

Long C-C bonds in di-diamantane ethane and hexaphenyl ethane

A normal alkane C-C bond is 1.54 Å long, but through the use of steric crowding in combination with favorable dispersion interactions, different stable alkanes with a C-C bond over 0.2 Å longer have been synthesized.[100–103] Despite appearing to have a partly broken C-C bond, some of these species are stable at room temperature. We first look at di-diamantane ethane,[100] shown in Figure 8, which is stable at room temperature with a bond distance of

Table 3: Binding energy and charge resonance states for a variety of mono-cation dimers. Experimental data is provided when available. The binding energy is in kcal/mol and the Charge Resonance energy is in eV.

	Binding energy					Charge Resonance		
molecule	NOCI	NOCI-MP2	MP2	ωB97x-V	Exp.	NOCI	NOCI-MP2	Exp.
aniline	3.3	14.7	16.1	14.02		1.17	1.02	1.12[a]
naphthalene	2.4	16.8	24.0	16.4	17.8[b]	1.12	1.00	1.05[c]
anthracene	-1.3	18.3	25.9	20.5	16.4[b]	1.05	0.92	
phenalenyl	-2.0	25.7	36.6	25.1		1.43	1.27	

[a] Values taken from reference 93
[b] Values taken from reference 94
[c] Values taken from reference 95

1.65 Å. This system has attracted considerable interest.[104–107]

Figure 8: A visualization of di-diamantane ethane at its equilibrium geometry, and the dissociation curve at the NOCI, red, and NOCI-MP2 level, blue.

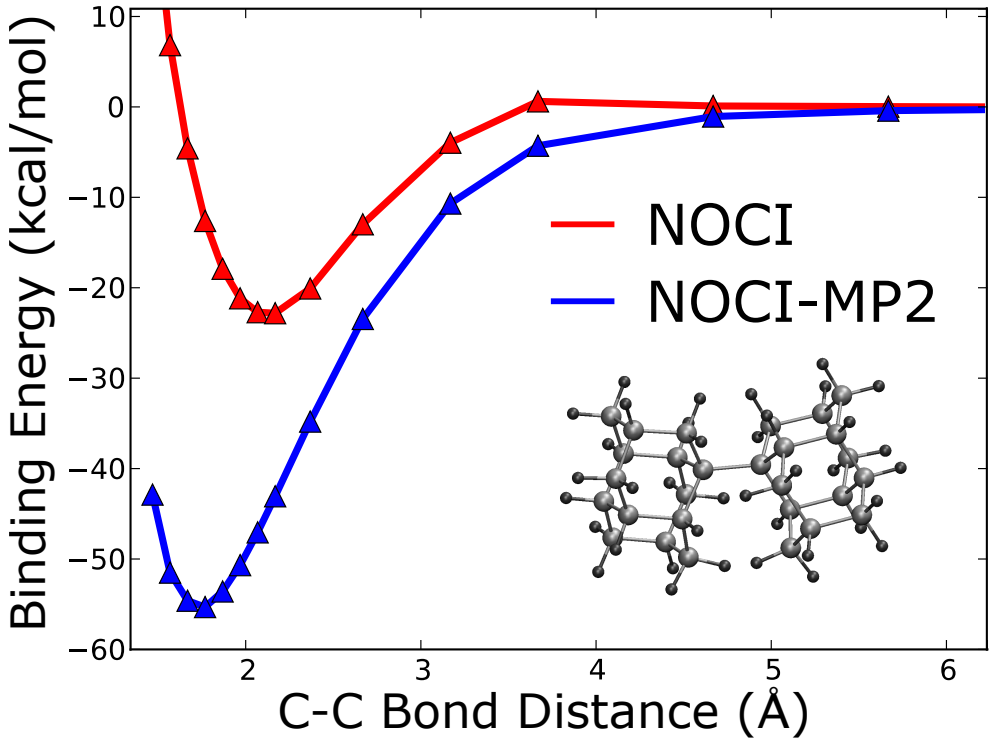

As one stretches the ethane C-C bond, the molecular wavefunction changes from being closed shell single reference to open-shell multireference where the two fragments contain a lone radical electron each. For both molecules we use the two radical and two ionic ALMO NOCI states, as employed in the previous subsection for the ethene dimer dication, and

TCNE dimer dianion. We use the same 6-31G(d,p) basis set that was used in reference 100 for di-diamantane ethane, and all geometry optimizations are done with the B97-D functional. At each point on the potential energy surface the geometry is optimized while constraining the central C-C bond distance. These geometries are given in the supporting information. The plot of the dissociation curve for di-diamantane ethane is in Figure 8.

The NOCI and NOCI-MP2 binding energies, after correcting for basis set superposition error (BSSE), are 23 and 56 kcal/mol, respectively. The NOCI-MP2 value is underbound by about 10 kcal/mol when compared to the dispersion corrected B3LYP-D results of 70.7 kcal/mol.,[100] or the ωB97M-V value of 65 kcal/mol.[105] Considering that neither of the DFT calculations were BSSE-corrected, and also that closer approach to the complete basis set limit would increase the NOCI-MP2 binding more significantly than the DFT binding (due to slower algebraic convergence of the wavefunction method with cardinal number of the basis,[108] we view this result as quite promising. By contrast, without damping the t amplitudes, the NOCI-MP2 binding energy is approximately 80 kcal/mol, which is significantly overbound compared to the DFT results, and would be further overbound upon improvement of the basis.

At the NOCI level (i.e. without dispersion interactions) di-diamantane ethane is still bound, which indicates that despite the steric repulsion of the bulky side groups, the electrons involved in the C-C single bond still strongly couple to each other. However, with the dispersion interactions included in NOCI-MP2 the molecule is significantly more bound. The attractive dispersion interactions outweigh the repulsive steric crowding for this system. However, the bond is still signficantly weaker than the roughly 90 kcal/mol value for the ethane C-C bond.

From equilibrium to dissociation, roughly 30 kcal/mol of relaxation energy occurs in the side groups of di-diamantane ethane. This side-group distortion associated with binding is why, in the NOCI case, the relaxed binding curve goes above 0.0 at 3.6 Å. If there was no side-group distortion due to steric hindrance during the bonding process the molecule would be

bound by almost 100 kcal/mol, larger than the roughly 90 kcal/mol bond dissociation energy of ethane. Other studies on di-diamantane ethane have pointed to the minimal geometry distortion in the diamantane side group upon formation of the C-C bond as the source of its stability.[74] The NOCI-MP2 calculations suggest that there is competition between steric repulsions that increase as the CC distance shortens, and attractive dispersion interactions that strengthen as the CC distance shortens. The result of this competition, in concert with the energetic cost of stretching the bonds (due to poorer electron pairing via spin coupling[109–111]) causes the optimal geometry of di-diamantane ethane to be 0.1 Å longer than the bond distance in ethane.

Figure 9: A model of hexaphenyl ethane, and the dissociation curve at the NOCI, red, and NOCI-MP2 level, blue.

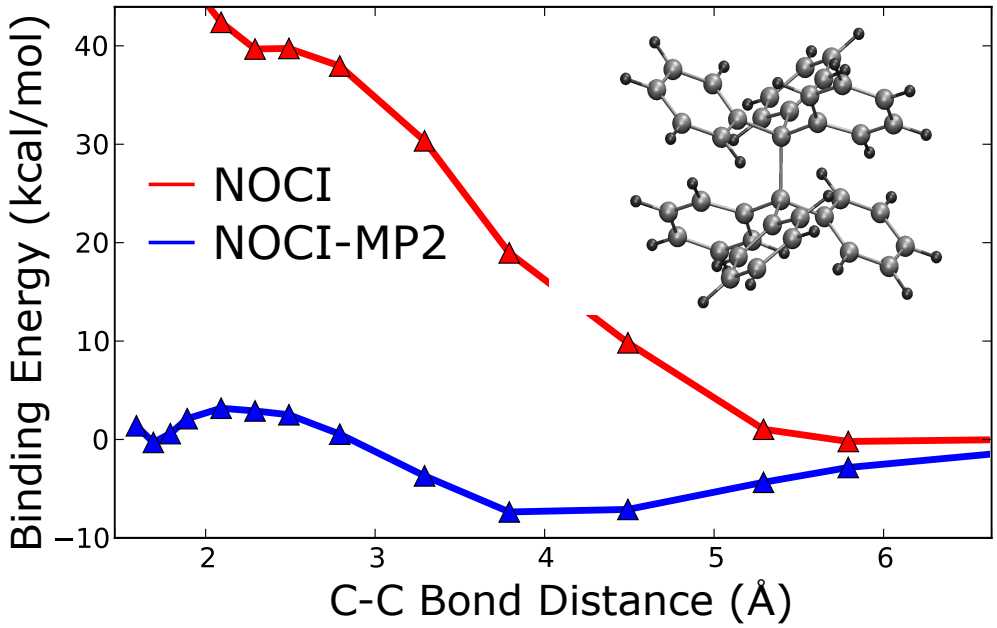

For hexaphenyl ethane, shown in Figure 9, we use the def2-TZVP basis set for all atoms except the two C atoms in the ethane C-C bond, for which we use the aug-cc-pVTZ basis set. This mixed basis description yields a total basis set size of 1388 functions. The quality of the ALMO NOCI determinants depend strongly on the quality of the basis set on the two C atoms involved in the bond that is being formed/broken. The accuracy of the ALMO determinants greatly improves with an increased basis set for the bonded atoms, and is less

important for the other atoms involved.

Unlike di-diamantane ethane, hexaphenyl ethane does not show a typical dissociation curve: as shown in Figure 9, the NOCI dissociation curve is unbound. Without the singles correction to the ALMO states, due to the non-Brillouin orbitals (i.e. they are not fully relaxed at the SCF level due to the ALMO constraint), the NOCI state doesn't even show an unstable minimum at the bonding distance. The shape of the NOCI curve shows the impact of steric hindrance and the relaxation energy gained in the triphenyl methyl radicals as they are pulled apart. At the bonded minimum, the bonded carbon atoms have slightly distorted tetrahedral geometry, with the distortion reflecting steric repulsions. Upon dissociation, the central radical carbon atom adopts a trigonal planar geometry, where, due to steric repulsion between phenyl groups, they twist out of the plane in a propeller-like structure. In this geometry the radical electron is able to couple better with the phenyl π electrons, which stabilizes the radical fragment.

With the inclusion of dispersion interactions via the NOCI-MP2 method, a weakly bound molecule is obtained. NOCI-MP2 is bound, with only by 1 kcal/mol of net binding at 1.69 Å. There is a more strongly bound second minimum (a bond stretch isomer) that appears around 4 Å. This isomer is calculated to be bound by 7.5 kcal/mol, and exhibits a much broader minimum. The relative heights of these two minima can change with the extent of damping of the small energy denominator t amplitudes. As we have seen in the previous examples, the chosen damping parameter, which is not optimized for this work, appears to lead to a slight underestimation of the dispersion energy.

The second minimum at 4 Åis strictly due to the dispersion interactions between the phenyl groups on the different methyl fragments: it is a broken bond that is stabilized by dispersion. A plot of the phenyl-phenyl distance between phenyl groups on the top and bottom methyl fragments, given in the Supporting Information, shows that the closest contact distance between them doesn't significantly change until after 4 Å. At this point, there starts to be a linear relationship between the central C-C bond distance and the closest

contact distance on the phenyl rings.

Based on these results, it is not surprising that hexaphenyl ethane has not been experimentally observed, since in this case the energy penalty required to distort the triphenyl methyl fragments in order to form the ethane bond is too large, and there is not enough compensating dispersion interaction to obtain a reasonably stable bond. In solution, the triphenyl methyl radical binds to a carbon atom in a phenyl ring over the formation of the ethane bond. The stability of the t-butyl version of hexaphenyl ethane in reference 100 appears to be due to two factors: the steric repulsions cause a C-phenyl interaction to be more difficult, and the increased dispersion interactions stabilize formation of the C-C bond.

Conclusion

Non-orthogonal configuration interaction with a second order perturbation correction (NOCI-MP2) is a flexible method that can describe some types of strong correlation with exceptionally compact wavefunctions. In this paper, we have presented working equations that enable an efficient NOCI-MP2 implementation, using the resolution of the identity (RI) approximation to the two-electron integrals. No individual term requires more computational time than RI-MP2, though there are multiple terms that do scale as RI-MP2 giving NOCI-MP2 a much larger prefactor. Using a set of conjugated organic molecules, we show that this prefactor no larger than 10 per off-diagonal element. In practice, the prefactor is smaller because in many cases some of the occupied orbital overlaps between different NOCI states are near zero. Overall, this implementation makes NOCI-MP2 comparable to low scaling multireference perturbation theory methods like CASPT2. The advantage of NOCI-MP2 is that a much smaller active space can often be used.

NOCI-MP2 is applied to a number of mono- and di-cation aromatic dimers. In these cases, we show that NOCI-MP2 can be combined with the absolutely localized MO (ALMO) method to create the set of NOCI determinants that rather directly represent covalent and

ionic diabatic states. We further show that the use of a singles correction to the MP2 energy brings yields relative energies that are in line with other multi-reference correlation theory methods like SF-EOM-CCSD and CASPT2. Inspection of the results shows that the coupling between the radical electrons, one on each monomer, is not enough to accurately describe the binding in the di-cation species. It is only after the addition of the ionic states, which account for 70% of the binding energy, that we get results which agree well with other theory and experiments. This illustrates that NOCI-MP2 has interpretative, as well as computational value when applied to molecules where the bonding is not already well-understood.

For aromatic mono-cation dimers (i.e. having a delocalized multi-center one-electron bond, rather than a two-electron bond), NOCI-MP2 shows itself to be capable of obtaining accurate charge resonance energies, using just two ALMO reference determinants. Currently we are limited to gas phase studies, but it is very promising that the results agree with available experimental results to about 2 kcal/mol. However, we note that this good agreement was only obtained after addressing the challenge of overbinding in NOCI-MP2, whose origin (small denominators) is the same as the cause of the well-known tendencies of MP2 to significantly overbind π-stack dimers between closed shell monomers. To damp the effects of small orbital differences, we apply a denominator level shift of 0.3 Hartree, taken from previous work on regularized orbital optimized MP2.[80] Inspecting our results suggests that slightly better accuracy might be possible by optimizing the damping parameter to a slightly smaller value. Systematic exploration of this optimization problem may be useful in the future.

We also presented NOCI-MP2 calculations for two bulky ethane derivatives: di-diamantane ethane and hexaphenyl ethane. Due to the minimal geometric relaxation in di-diamantane ethane, the dissociation curve is representative of a typical single bond, with or without the dispersion interactions. Upon inclusion of dispersion interactions via NOCI-MP2, the binding energy is only 30 kcal/mol less stable than the ethane C-C bond. This relatively strong bond results from the strong dispersion interactions combined with relatively small geometric distortion in the diamantane side groups upon formation of a C-C bond that is

only stretched by 0.1 Å relative to ethane. For hexaphenyl ethane the geometric distortion is much more significant, such that at the NOCI level the system is unbound.

The work presented here shows the promise of the NOCI-MP2 method for applications to large molecular systems. The largest calculations employed 1388 basis functions, and were successful in treating systems that show strong correlation. The NOCI-MP2 method is especially useful in cases where the set of non-aufbau configurations (i.e. diabatic states) used in the non-orthogonal CI is well defined. This was accomplished here using covalent and ionic ALMO determinants. All of the potential energy surfaces presented here were done with either rigid monomers or using a different method to perform constrained geometry optimization. In the future it would be greatly beneficial (though also quite non-trivial) to implement analytical gradients for NOCI-MP2.

Acknowledgement

This research was supported by the Director, Office of Science, Office of Basic Energy Sciences, of the U.S. Department of Energy under Contract No. DE-AC02-05CH11231.

References

(1) Goerigk, L.; Grimme, S. A thorough benchmark of density functional methods for general main group thermochemistry, kinetics, and noncovalent interactions. *Phys. Chem. Chem. Phys.* **2011**, *13*, 6670–6688.

(2) Peverati, R.; Truhlar, D. G. Quest for a universal density functional: the accuracy of density functionals across a broad spectrum of databases in chemistry and physics. *Phil. Trans. R. Soc. A* **2014**, *372*.

(3) Mardirossian, N.; Head-Gordon, M. ω B97M-V: A combinatorially optimized, range-separated hybrid, meta-GGA density functional with VV10 nonlocal correlation. *J. Chem. Phys.* **2016**, *144*, 214110.

(4) Goerigk, L.; Hansen, A.; Bauer, C.; Ehrlich,; Stephan,; Najibi, A.; Grimme, S. A look at the density functional theory zoo with the advanced GMTKN55 database for general main group thermochemistry, kinetics and noncovalent interactions. *Phys. Chem. Chem. Phys.* **2017**, *19*, 32184–32215.

(5) Mardirossian, N.; Head-Gordon, M. Thirty years of density functional theory in computational chemistry: an overview and extensive assessment of 200 density functionals. *Molecular Physics* **2017**, *115*, 2315–2372.

(6) Cohen, A. J.; Mori-Sanchez, P.; Yang, W. T. Challenges for Density Functional Theory. *Chem. Rev.* **2012**, *112*, 289–320.

(7) Krylov, A. I.; Sherrill, C. D.; Byrd, E. F.; Head-Gordon, M. Size-consistent wave functions for nondynamical correlation energy: The valence active space optimized orbital coupled-cluster doubles model. *J. Chem. Phys.* **1998**, *109*, 10669–10678.

(8) Small, D. W.; Head-Gordon, M. Post-Modern Valence Bond Theory for Strongly Correlated Electron Spins. *Phys. Chem. Chem. Phys.* **2011**, *13*, 19285–19297.

(9) Krylov, A. I. Size-Consistent Wave Functions for Bond-Breaking: The Equation-of-Motion Spin-Flip Model. *Chem. Phys. Lett.* **2001**, *338*, 375–384.

(10) Serrano-Andres, L.; Merchán, M.; Lindh, R. Computation of Conical Intersections by Using Perturbation Techniques. *J. Chem. Phys.* **2005**, *122*, 104107.

(11) Alguire, E.; Subotnik, J. E. Diabatic couplings for charge recombination via Boys localization and spin-flip configuration interaction singles. *J. Chem. Phys.* **2011**, *135*, 044114.

(12) Hanrath, M. Multi-reference coupled-cluster study of the ionic-neutral curve crossing LiF. *Mol. Phys.* **2008**, *106*, 1949–1957.

(13) Malrieu, J. P.; Caballol, R.; Calzado, C. J.; De Graaf, C.; Guihéry, N. Magnetic Interactions in Molecules and Highly Correlated Materials: Physical Content, Analytical Derivation, and Rigorous Extraction of Magnetic Hamiltonians. *Chem. Rev.* **2013**, *114*, 429–492.

(14) Mayhall, N. J.; Head-Gordon, M. Computational quantum chemistry for single Heisenberg spin couplings made simple: Just one spin flip required. *J. Chem. Phys.* **2014**, *141*, 134111.

(15) Mayhall, N. J.; Head-Gordon, M. Computational Quantum Chemistry for Multiple-Site Heisenberg Spin Couplings Made Simple: Still Only One Spin-Flip Required. *J. Phys. Chem. Lett.* **2015**, *6*, 1982–1988.

(16) Rajca, A. Organic Diradicals and Polyradicals - from Spin Coupling to Magnetism. *Chem. Rev.* **1994**, *94*, 871–893.

(17) Slipchenko, L. V.; Krylov, A. I. Singlet-Triplet Gaps in Diradicals by the Spin-Flip Approach: A Benchmark Study. *J. Chem. Phys.* **2002**, *117*, 4694–4708.

(18) Shao, Y.; Head-Gordon, M.; Krylov, A. I. The Spin-Flip Approach within Time-Dependent Density Functional Theory: Theory and Applications to Diradicals. *J. Chem. Phys.* **2003**, *118*, 4807–4818.

(19) Chan, G. K. L.; Head-Gordon, M. Highly correlated calculations with a polynomial cost algorithm: A study of the density matrix renormalization group. *J. Chem. Phys.* **2002**, *116*, 4462–4476.

(20) Mitrushenkov, A.; Linguerri, R.; Palmieri, P.; Fano, G. Quantum chemistry using the density matrix renormalization group II. *J. Chem. Phys.* **2003**, *119*, 4148–4158.

(21) Chan, G. K.-L.; Sharma, S. The density matrix renormalization group in quantum chemistry. *Annu. Rev. Phys. Chem.* **2011**, *62*, 465–481.

(22) Booth, G. H.; Thom, A. J. W.; Alavi, A. Fermion Monte Carlo without fixed nodes: A game of life, death, and annihilation in Slater determinant space. *J. Chem. Phys.* **2009**, *131*, 054106.

(23) Cleland, D.; Booth, G. H.; Alavi, A. Communications: Survival of the fittest: Accelerating convergence in full configuration-interaction quantum Monte Carlo. *J. Chem. Phys.* **2010**, *132*, 041103.

(24) Li Manni, G.; Smart, S. D.; Alavi, A. Combining the Complete Active Space Self-Consistent Field Method and the Full Configuration Interaction Quantum Monte Carlo within a Super-CI Framework, with Application to Challenging Metal-Porphyrins. *J. Chem. Theor. Comput.* **2016**, *12*, 1245–1258.

(25) Schriber, J. B.; Evangelista, F. A. Communication: An adaptive configuration interaction approach for strongly correlated electrons with tunable accuracy. *J. Chem. Phys.* **2016**, *144*, 161106.

(26) Tubman, N. M.; Lee, J.; Takeshita, T. Y.; Head-Gordon, M.; Whaley, K. B. A deterministic alternative to the full configuration interaction quantum Monte Carlo method. *J. Chem. Phys.* **2016**, *145*, 044112.

(27) Holmes, A. A.; Tubman, N. M.; Umrigar, C. J. Heat-Bath Configuration Interaction: An Efficient Selected Configuration Interaction Algorithm Inspired by Heat-Bath Sampling. *J. Chem. Theor. Comput.* **2016**, *12*, 3674–3680.

(28) Szalay, P. G.; Mueller, T.; Gidofalvi, G.; Lischka, H.; Shepard, R. Multiconfiguration Self-Consistent Field and Multireference Configuration Interaction Methods and Applications. *Chem. Rev.* **2012**, *112*, 108–181.

(29) Roos, B. O.; Taylor, P. E. M.; Siegbahn, A Complete Active Space SCF Method (CASSCF) Using a Density Matrix Formulated Super-CI Approach. *Chem. Phys.* **1980**, *48*, 157–173.

(30) Roos, B. O. The Complete Active Space Self-Consistent Field Method and its Applications in Electronic Structure Calculations. *Adv. Chem. Phys.* **1987**, *69*, 399–445.

(31) Vogiatzis, K. D.; Li Manni, G.; Stoneburner, S. J.; Ma, D.; Gagliardi, L. Systematic Expansion of Active Spaces beyond the CASSCF Limit: A GASSCF/SplitGAS Benchmark Study. *Journal of chemical theory and computation* **2015**, *11*, 3010–3021.

(32) Malmqvist, P. Å.; Rendell, A.; Roos, B. O. The Restricted Active Space Self-Consistent-Field Method, Implemented with a Split Graph Unitary Group Approach. *J. Phys. Chem.* **1990**, *94*, 5477–5482.

(33) Casanova, D.; Head-Gordon, M. Restricted Active Space Spin-Flip Configuration Interaction Approach: Theory, Implementation and Examples. *Phys. Chem. Chem. Phys.* **2009**, *11*, 9779–9790.

(34) Zimmerman, P. M.; Bell, F.; Goldey, M.; Bell, A. T.; Head-Gordon, M. Restricted Active Space Spin-Flip Configuration Interaction: Theory and Examples for Multiple Spin Flips with Odd Numbers of Electrons. *J. Chem. Phys.* **2012**, *137*, 164110.

(35) Mayhall, N. J.; Head-Gordon, M. Increasing Spin-flips and Decreasing Cost: Perturbative Corrections for External Singles to the Complete Active Space Spin Flip Model for Low-Lying Excited States and Strong Correlation. *J. Chem. Phys.* **2014**, *141*, 044112.

(36) Wu, W.; Su, P.; Shaik, S.; Hiberty, P. C. Classical Valence Bond Approach by Modern Methods. *Chem. Rev.* **2011**, *111*, 7557–7593.

(37) Su, P.; Wu, W. Ab initio nonorthogonal valence bond methods. *WIREs Comput. Mol. Sci.* **2013**, *3*, 56–68.

(38) Gerratt, J.; Cooper, D. L.; Karadakov, P. B.; Raimondi, M. Modern Valence Bond Theory. *Chem. Soc. Rev.* **1997**, *26*, 87–100.

(39) Small, D. W.; Lawler, K. V.; Head-Gordon, M. Coupled Cluster Valence Bond Method: Efficient Computer Implementation and Application to Multiple Bond Dissociations and Strong Correlations in the Acenes. *J. Chem. Theor. Comput.* **2014**, *10*, 2027–2040.

(40) Hiberty, P. C.; Humbel, S.; Byrman, C. P.; van Lenthe, J. H. Compact Valence Bond Functions with Breathing Orbitals: Application to the Bond Dissociation Energies of F2 and FH. *J. Chem. Phys.* **1994**, *101*, 5969–5976.

(41) Hiberty, P. C.; Shaik, S. Breathing-Orbital Valence Bond Method–A Modern Valence

Bond Method That Includes Dynamic Correlation. *Theor. Chem. Acc.* **2002**, *108*, 255–272.

(42) Broer, R.; Nieuwpoort, W. Broken orbital symmetry and the description of valence hole states in the tetrahedral CRO4(2-) ANION. *Theor. Chim. Acta* **1988**, *73*, 405–418.

(43) Broer, R.; Nieuwpoort, W. Hole localization and symmetry breaking. *J. Mol. Struct. Theochem* **1999**, *458*, 19–25.

(44) Broer, R.; Hozoi, L.; Nieuwpoort, W. Non-orthogonal approaches to the study of magnetic interactions. *Mol. Phys.* **2003**, *101*, 233–240.

(45) Thom, A. J.; Head-Gordon, M. Hartree-Fock Solutions As a Quasidiabatic Basis for Nonorthogonal Configuration Interaction. *J. Chem. Phys.* **2009**, *131*, 124113.

(46) Sundstrom, E. J.; Head-Gordon, M. Non-Orthogonal Configuration Interaction for the Calculation of Multielectron Excited States. *J. Chem. Phys.* **2014**, *140*, 114103.

(47) Thom, A.; Head-Gordon, M. Locating Multiple Self-Consistent Field Solutions: An Approach Inspired by Metadynamics. *Phys. Rev. Lett.* **2008**, *101*, 193001.

(48) Mayhall, N. J.; Horn, P. R.; Sundstrom, E. J.; Head-Gordon, M. Spin-Flip Non-Orthogonal Configuration Interaction: A Variational and Almost Black-Box Method for Describing Strongly Correlated Molecules. *Phys. Chem. Chem. Phys.* **2014**, *16*, 22694–22705.

(49) Bartlett, R. J.; Musiał, M. Coupled-Cluster Theory in Quantum Chemistry. *Rev. Mod. Phys.* **2007**, *79*, 291.

(50) Møller, C.; Plesset, M. S. Note on an Approximation Treatment for Many-Electron Systems. *Phys. Rev.* **1934**, *46*, 618.

(51) Mahapatra, U. S.; Datta, B.; Mukherjee, D. Molecular Applications of a Size-Consistent State-Specific Multireference Perturbation Theory with Relaxed Model-Space Coefficients. *J. Phys. Chem. A* **1999**, *103*, 1822–1830.

(52) Mahapatra, U. S.; Datta, B.; Mukherjee, D. A state-specific multi-reference coupled cluster formalism with molecular applications. *Mol. Phys.* **1998**, *94*, 157–171.

(53) Chaudhuri, R. K.; Freed, K. F.; Hose, G.; Piecuch, P.; Kowalski, K.; Włoch, M.; Chattopadhyay, S.; Mukherjee, D.; Rolik, Z.; Szabados, Á.; Tóth, G.; Surján, P. R. Comparison of low-order multireference many-body perturbation theories. *J. Chem. Phys.* **2005**, *122*, 134105.

(54) Ghosh, P.; Chattopadhyay, S.; Jana, D.; Mukherjee, D. State-specific Multi-reference Perturbation Theories with Relaxed Coefficients: Molecular Applications. *Int. J. Mol. Sci.* **2002**, *3*, 733–754.

(55) Chen, Z.; Song, J.; Shaik, S.; Hiberty, P. C.; Wu, W. Valence Bond Perturbation Theory. A Valence Bond Method That Incorporates Perturbation Theory. *J. Phys. Chem. A* **2009**, *113*, 11560–11569.

(56) Chen, Z.; Chen, X.; Ying, F.; Gu, J.; Zhang, H.; Wua, W. Nonorthogonal orbital based n-body reduced density matrices and their applications to valence bond theory. III. Second-order perturbation theory using valence bond self-consistent field function as reference. *J. Chem. Phys.* **2014**, *141*, 134118.

(57) Andersson, K.; Malmqvist, P. Å.; Roos, B. O. Second-Order Perturbation Theory with a Complete Active Space Self-Consistent Field Reference Function. *J. Chem. Phys.* **1992**, *96*, 1218–1226.

(58) Pulay, P. A perspective on the CASPT2 method. *Int. J. Quantum Chem.* **2011**, *111*, 3273–3279.

(59) Finley, J.; Malmqvist, P. Å.; Roos, B. O.; Serrano-Andrés, L. The Multi-State CASPT2 Method. *Chem. Phys. Lett.* **1998**, *288*, 299–306.

(60) Angeli, C.; Cimiraglia, R.; Evangelisti, S.; Leininger, T.; Malrieu, J.-P. Introduction of n-electron Valence States for Multireference Perturbation Theory. *J. Chem. Phys.* **2001**, *114*, 10252–10264.

(61) Angeli, C.; Pastore, M.; Cimiraglia, R. New perspectives in multireference perturbation theory: the n-electron valence state approach. *Theor. Chem. Acc.* **2007**, *117*, 743–754.

(62) Mahapatra, U. S.; Datta, B.; Mukherjee, D. Development of a Size-Consistent State-Specific Multireference Perturbation Theory with Relaxed Model-Space Coefficients. *Chem. Phys. Lett.* **1999**, *299*, 42–50.

(63) Mbote, Y. E. B.; Khait, Y. G.; Hardel, C.; Hoffmann, M. R. Multireference Generalized Van Vleck Perturbation Theory (GVVPT2) Study of the NCO+ HCNO Reaction: Insight into Intermediates. *J. Phys. Chem. A* **2010**, *114*, 8831–8836.

(64) Khait, Y. G.; Song, J.; Hoffmann, M. R. Explication and revision of generalized Van Vleck perturbation theory for molecular electronic structure. *J. Chem. Phys.* **2002**, *117*, 4133–4145.

(65) Malrieu, J.; Durand, P.; Daudey, J. Intermediate Hamiltonians as a new class of effective Hamiltonians. *J. Phys. A Math. Gen.* **1985**, *18*, 809.

(66) Ayala, P. Y.; Schlegel, H. B. A Nonorthogonal Ci Treatment of Symmetry Breaking in Sigma Formyloxyl Radical. *J. Chem. Phys.* **1998**, *108*, 7560–7567.

(67) Yost, S. R.; Kowalczyk, T.; Van Voorhis, T. A Multireference Perturbation Method Using Non-Orthogonal Hartree-Fock Determinants for Ground and Excited States. *J. Chem. Phys.* **2013**, *139*, 174104.

(68) Yost, S. R.; Head-Gordon, M. Size consistent formulations of the perturb-then-diagonalize Møller-Plesset perturbation theory correction to non-orthogonal configuration interaction. *J. Chem. Phys.* **2016**, *145*, 054105.

(69) Wu, W.; Zhang, H.; Braida, B.; Shaik, S.; Hiberty, P. C. The V state of ethylene: valence bond theory takes up the challenge. *Theor. Chem. Acc.* **2014**, *133*.

(70) Weigend, F.; Häser, M.; Patzelt, H.; Ahlrichs, R. RI-MP2: optimized auxiliary basis sets and demonstration of efficiency. *Chem. Phys. Let.* **1998**, *294*, 143–152.

(71) Vahtras, O.; Almlöf, J.; Feyereisen, M. Integral approximations for LCAO-SCF calculations. *Chem. Phys. Let.* **1993**, *213*, 514–518.

(72) Miller, J. S. Long, Multicenter Bonding: A New Concept for Supramolecular Materials. *Chem. Eur. J.* **2015**, *21*, 9302–9305.

(73) Zhang, D.-W.; Tian, J.; Chen, L.; Zhang, L.; Li, Z.-T. Dimerization of Conjugated Radical Cations: An Emerging Non-Covalent Interaction for Self-Assembly. *Chem. Asian J.* **2015**, *10*, 56–68.

(74) Cho, D.; Ikabata, Y.; Yoshikawa, T.; Lee, J.; Nakai, H. Theoretical Study of Extremely Long yet Stable Carbon-Carbon Bonds: Effect of Attractive C center dot center dot center dot H Interactions and Small Radical Stabilization of Diamondoids. *Bull. Chem. Soc. Jpn.* **2015**, *88*, 1636–1641.

(75) Wagner, J. P.; Schreiner, P. R. London Dispersion in Molecular Chemistry-Reconsidering Steric Effects. *Angew. Chem. Int. Ed.* **2015**, *54*, 12274–12296.

(76) King, H. F.; Stanton, R. E.; Kim, H.; Wyatt, R. E.; Parr, R. G. Corresponding orbitals and the nonorthogonality problem in molecular quantum mechanics. *J. Chem. Phys.* **1967**, *47*, 1936–1941.

(77) Distasio, R.; Steele, R.; Rhee, Y.; Shao, Y.; Head-Gordon, M. An improved algorithm for analytical gradient evaluation in resolution-of-the-identity second-order Moller-Plesset perturbation theory: Application to alanine tetrapeptide conformational analysis. *J. Comput. Chem.* **2007**, *28*, 839–856.

(78) Goldey, M.; DiStasio, R. A.; Shao, Y. H.; Head-Gordon, M. Shared memory multiprocessing implementation of resolution-of-the-identity second-order Moller-Plesset perturbation theory with attenuated and unattenuated results for intermolecular interactions between large molecules. *Mol. Phys.* **2014**, *112*, 836–843.

(79) Shao, Y. et al. Advances in Molecular Quantum Chemistry Contained in the Q-Chem 4 Program Package. *Mol. Phys.* **2015**, *113*, 184–215.

(80) Stück, D.; Head-Gordon, M. Regularized Orbital-Optimized Second-Order Perturbation Theory. *J. Chem. Phys.* **2013**, *139*, 244109.

(81) Mota, F.; Miller, J. S.; Novoa, J. J. Comparative analysis of the multicenter, long bond in [TCNE]·- and phenalenyl radical dimers: a unified description of multicenter, long bonds. *J. Am. Chem. Soc.* **2009**, *131*, 7699–7707.

(82) Capdevila-Cortada, M.-a.; Ribas-Arino, J.; Novoa, J. J. Assessing the Performance of CASPT2 and DFT Methods for the Description of Long, Multicenter Bonding in Dimers between Radical Ions. *J. Chem. Theory Comput.* **2014**, *10*, 650–658.

(83) Capdevila-Cortada, M.; Ribas-Arino, J.; Chaumont, A.; Wipff, G.; Novoa, J. J. Formation of Long, Multicenter pi-[TCNE](2)(2-) Dimers in Solution: Solvation and Stability Assessed through Molecular Dynamics Simulations. *Chem. Eur. J.* **2016**, *22*, 17035–17044.

(84) Stoll, H.; Wagenblast, G.; Preuß, H. On the use of local basis sets for localized molecular orbitals. *Theor. Chim. Acta.* **1980**, *57*, 169–178.

(85) Khaliullin, R. Z.; Head-Gordon, M.; Bell, A. T. An efficient self-consistent field method for large systems of weakly interacting components. *J. Chem. Phys.* **2006**, *124*, 204105.

(86) Horn, P. R.; Sundstrom, E. J.; Baker, T. A.; Head-Gordon, M. Unrestricted absolutely localized molecular orbitals for energy decomposition analysis: Theory and applications to intermolecular interactions involving radicals. *J. Chem. Phys.* **2013**, *138*, 134119.

(87) Chai, J. D.; Head-Gordon, M. Long-range corrected hybrid density functionals with damped atom-atom dispersion corrections. *Phys. Chem. Chem. Phys.* **2008**, *10*, 6615–6620.

(88) Shaik, S.; Danovich, D.; Silvi, B.; Lauvergnat, D. L.; Hiberty, P. C. Charge-shift bonding - A class of electron-pair bonds that emerges from valence bond theory and is supported by the electron localization function approach. *Chem. Eur. J.* **2005**, *11*, 6358–6371.

(89) Braïda, B.; Hiberty, P. C. The essential role of charge-shift bonding in hypervalent prototype XeF2. *Nat. Chem.* **2013**, *5*, 417–422.

(90) Yamada, J.-i.; Sugimoto, T. *TTF Chemistry: Fundamentals and Applications of Tetrathiafulvalene*; Springer, 2004.

(91) Bendikov, M.; Wudl, F.; Perepichka, D. F. Tetrathiafulvalenes, oligoacenenes, and their buckminsterfullerene derivatives: The brick and mortar of organic electronics. *Chem. Rev.* **2004**, *104*, 4891–4946.

(92) Ishiguro, T.; Yamaji, K.; Saito, G. *Organic superconductors*; Springer Science & Business Media, 2012; Vol. 88.

(93) Roy, M.; Kim, K. K.; Nam, S. H.; Alauddin, M.; Song, J. K.; Park, S. M. Charge resonance structure of aniline dimer cation. *Int. J. Mass Spectrom.* **2016**, *402*, 66–72.

(94) Meot-Ner, M. Dimer cations of polycyclic aromatics. Experimental bonding energies and resonance stabilization. *J. Phys. Chem* **1980**, *84*, 2724–2728.

(95) Fujiwara, T.; Lim, E. C. Binding energies of the neutral and ionic clusters of naphthalene in their ground electronic states. *J. Phys. Chem. A* **2003**, *107*, 4381–4386.

(96) Mardirossian, N.; Head-Gordon, M. omega B97X-V: A 10-parameter, range-separated hybrid, generalized gradient approximation density functional with nonlocal correlation, designed by a survival-of-the-fittest strategy. *Phys. Chem. Chem. Phys.* **2014**, *16*, 9904–9924.

(97) Sinnokrot, M.; Sherrill, C. Highly accurate coupled cluster potential energy curves for the benzene dimer: Sandwich, T-shaped, and parallel-displaced configurations. *J. Phys. Chem. A* **2004**, *108*, 10200–10207.

(98) Hobza, P.; Sponer, J. Toward true DNA base-stacking energies: MP2, CCSD(T), and complete basis set calculations. *J. Am. Chem. Soc.* **2002**, *124*, 11802–11808.

(99) Bachorz, R. A.; Bischoff, F. A.; Höfener, S.; Klopper, W.; Ottiger, P.; Leist, R.; Frey, J. A.; Leutwyler, S. Scope and limitations of the SCS-MP2 method for stacking and hydrogen bonding interactions. *Phys. Chem. Chem. Phys.* **2008**, *10*, 2758–2766.

(100) Schreiner, P. R.; Chernish, L. V.; Gunchenko, P. A.; Tikhonchuk, E. Y.; Hausmann, H.; Serafin, M.; Schlecht, S.; Dahl, J. E.; Carlson, R. M.; Fokin, A. A. Overcoming lability of extremely long alkane carbon-carbon bonds through dispersion forces. *Nature* **2011**, *477*, 308–311.

(101) Flamm-ter Meer, M.; Beckhaus, H.-D.; Peters, K.; von Schnering, H.-G.; Rüchardt, C. Thermolabile hydrocarbons. XXVII: 2, 3-Di-1-adamantyl-2, 3-dimethylbutane; long bonds and low thermal stability. *Chem. Ber.* **1985**, *118*, 4665–4673.

(102) Fokin, A. A.; Chernish, L. V.; Gunchenko, P. A.; Tikhonchuk, E. Y.; Hausmann, H.; Serafin, M.; Dahl, J. E.; Carlson, R. M.; Schreiner, P. R. Stable alkanes containing very long carbon–carbon bonds. *J. Am. Chem. Soc.* **2012**, *134*, 13641–13650.

(103) Kahr, B.; Van Engen, D.; Mislow, K. Length of the ethane bond in hexaphenylethane and its derivatives. *J. Am. Chem. Soc.* **1986**, *108*, 8305–8307.

(104) Meitei, O. R.; Hesselmann, A. Intramolecular Interactions in Sterically Crowded Hydrocarbon Molecules. *J. Comput. Chem.* **2017**, *38*, 2500–2508.

(105) Levine, D. S.; Head-Gordon, M. Energy decomposition analysis of single bonds within Kohn-Sham density functional theory. *Proc. Natl. Acad. Sci. U. S. A.* **2017**, *114*, 12649–12656.

(106) Fokin, A. A. et al. Intramolecular London Dispersion Interaction Effects on Gas-Phase and Solid-State Structures of Diamondoid Dimers. *J. Am. Chem. Soc.* **2017**, *139*, 16696–16707.

(107) Ishigaki, Y.; Shimajiri, T.; Takeda, T.; Katoono,; Ryo,; Suzuki, T. Longest C-C Single Bond among Neutral Hydrocarbons with a Bond Length beyond 1.8 angstrom. *CHEM* **2018**, *4*, 795–806.

(108) Helgaker, T.; Klopper, W.; Tew, D. Quantitative quantum chemistry. *Mol. Phys.* **2008**, *106*, 2107–2143.

(109) Ruedenberg, K. The Physical Nature of the Chemical Bond. *Rev. Mod. Phys.* **1962**, *34*, 326–376.

(110) Schmidt, M. W.; Ivanic, J.; Ruedenberg, K. Covalent bonds are created by the drive of electron waves to lower their kinetic energy through expansion. *J. Chem. Phys.* **2014**, *140*, 204104.

(111) Levine, D. S.; Horn, P. R.; Mao, Y.; Head-Gordon, M. Variational Energy Decomposition Analysis of Chemical Bonding. 1. Spin-Pure Analysis of Single Bonds. *J. Chem. Theor. Comput.* **2016**, *12*, 4812–4820.

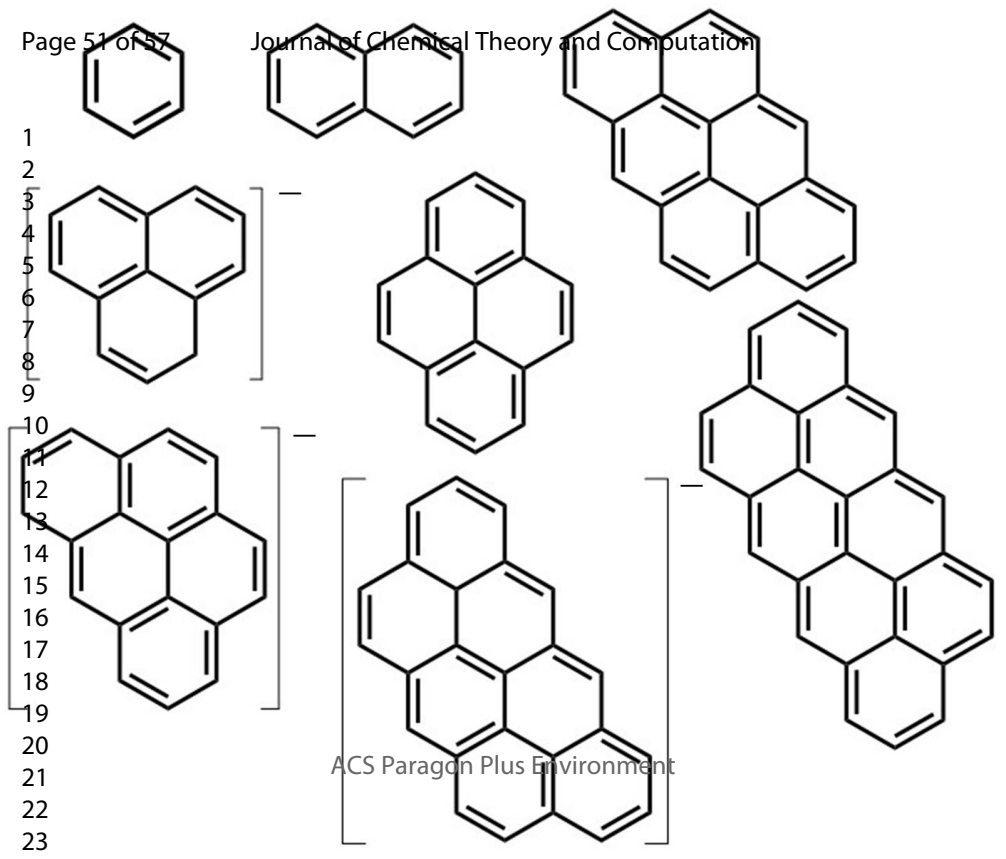

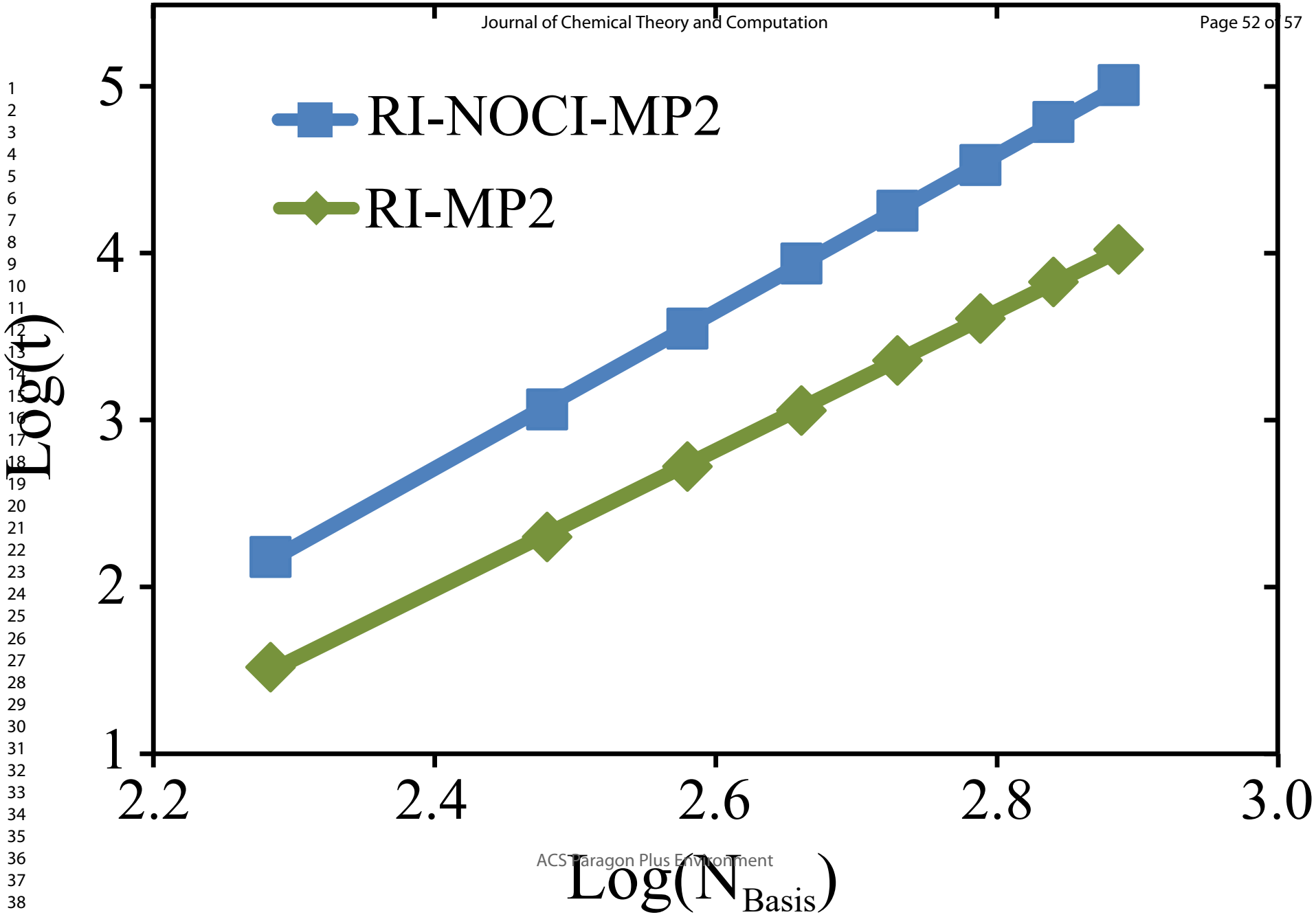

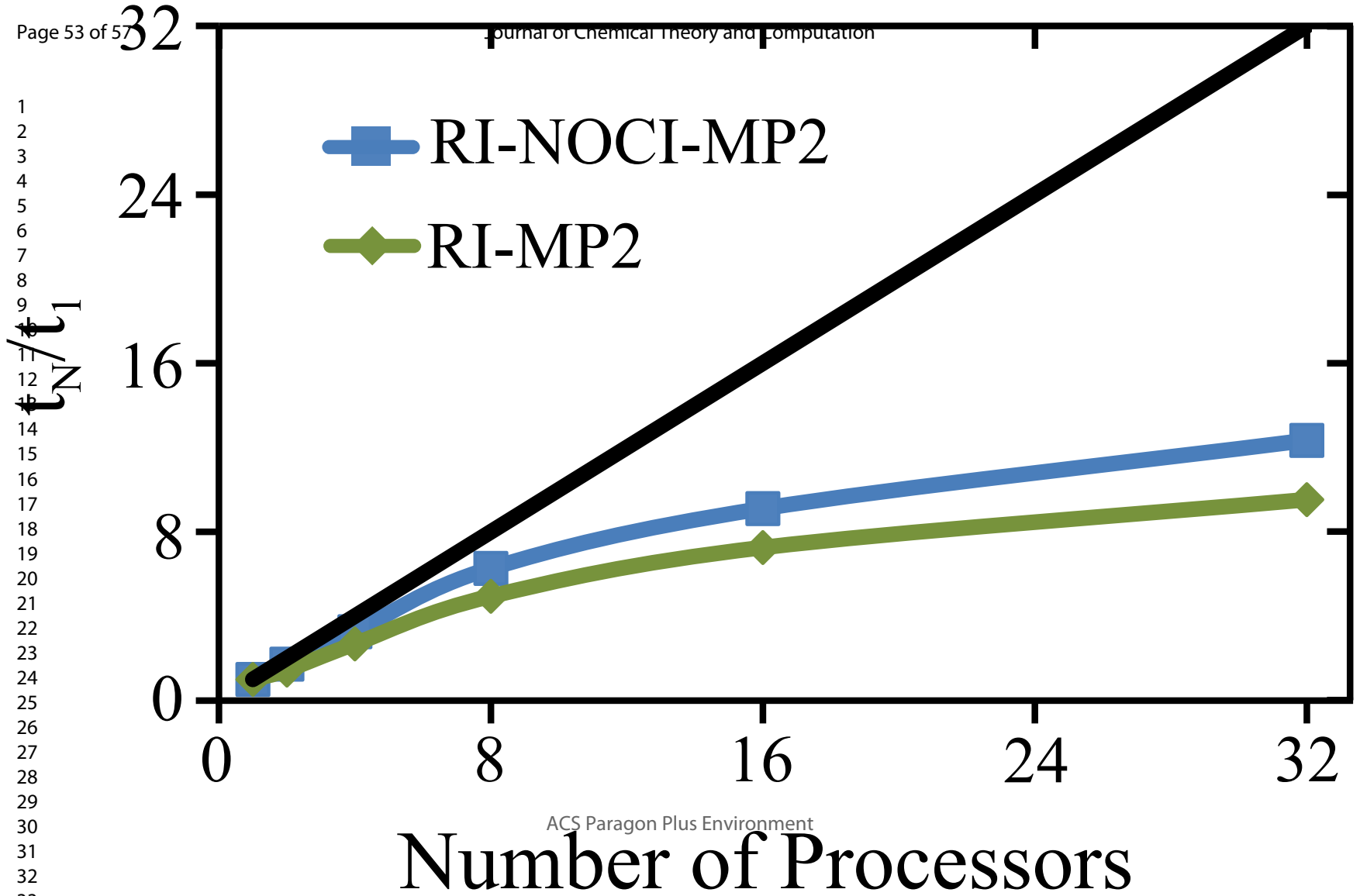
RI-NOCI-MP2
RI-MP2
t_N/t_1
0
8
16
24
32
0
8
16
24
32
Number of Processors

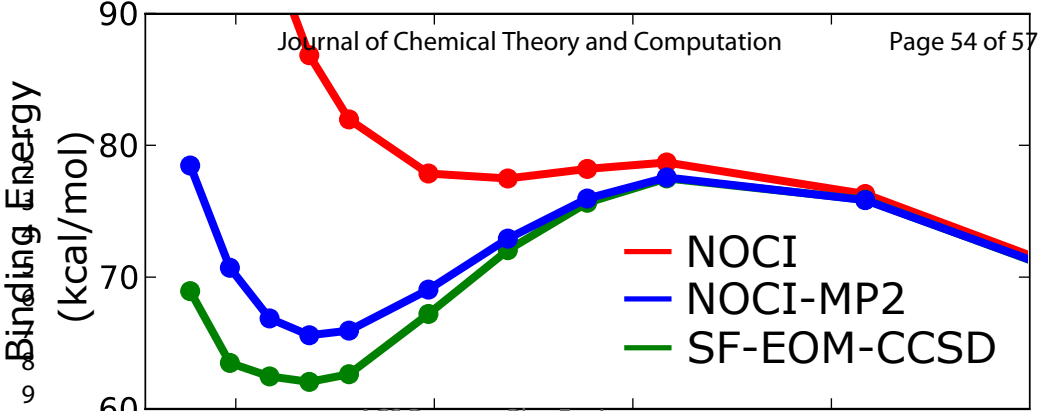

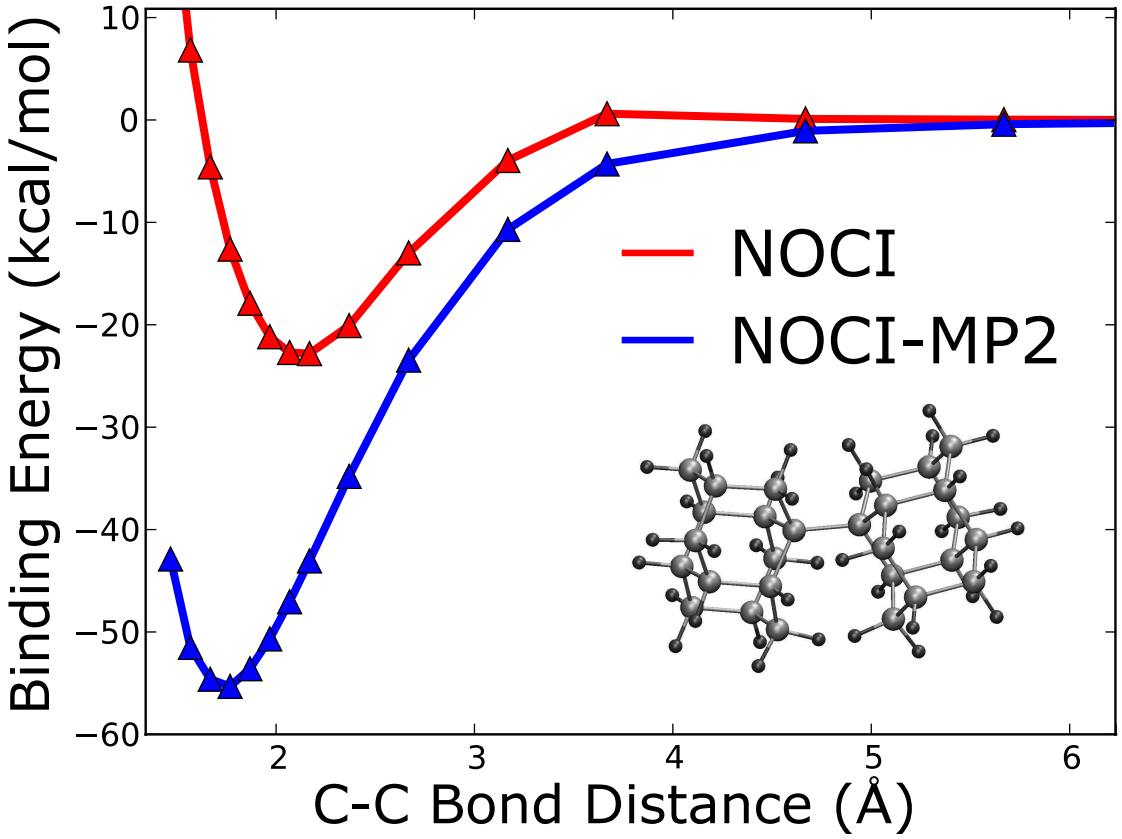
Binding Energy (kcal/mol)
10
0
−10
−20
−30
−40
−50
−60
2
3
4
5
6
C-C Bond Distance (Å)
NOCI
NOCI-MP2

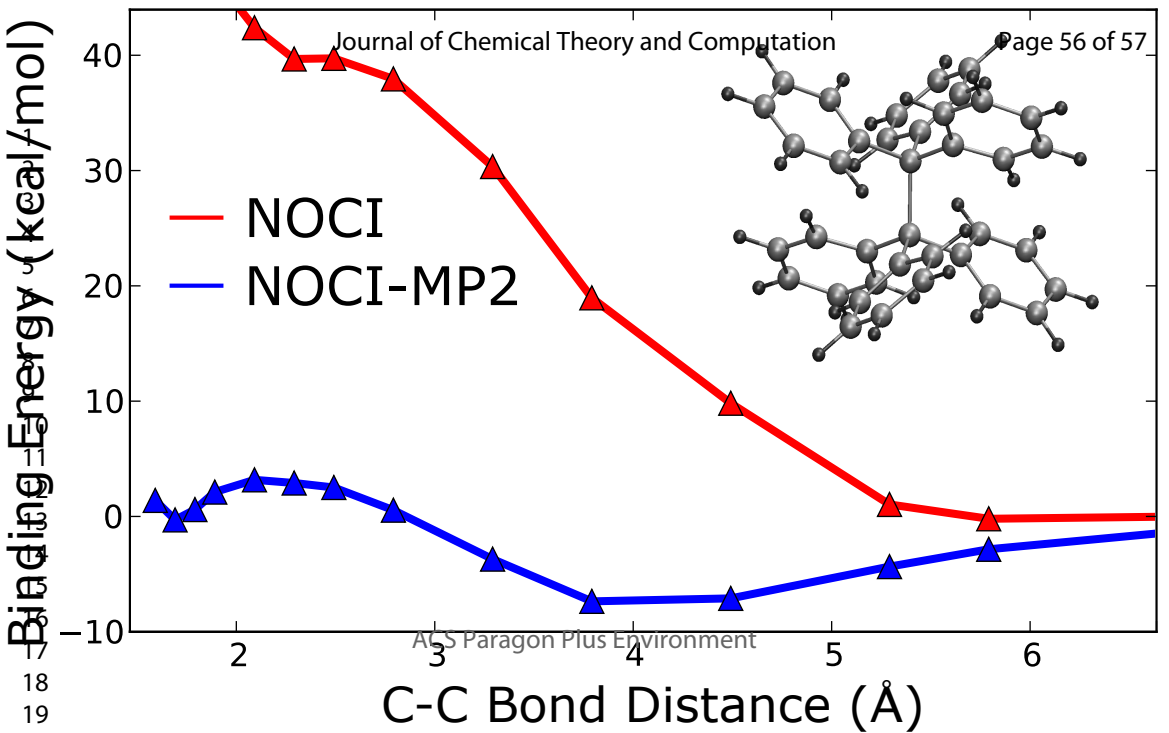

$$H = H_{\mathrm{NOCI}} - \sum_{ia} \frac{F_{ia}^2}{\Delta\varepsilon_i^a} - \sum_{ijab} \frac{\langle ij||ab\rangle^2}{\Delta\varepsilon_{ij}^{ab}}$$

$$\langle ij|ab\rangle \approx \sum_P B_{ia}^P B_{jb}^P$$

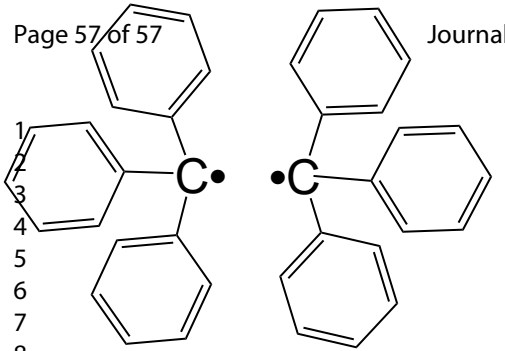

Covalent

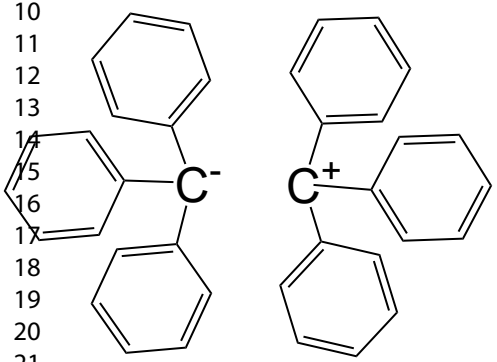

Ionic